CHALMERS

Comparison of Control Approaches for Permanent Magnet Motors

Master of Science Thesis

EMIL KLINTBERG

Department of Energy and Environment
Division of Electric Power Engineering
CHALMERS UNIVERSITY OF TECHNOLOGY
Göteborg, Sweden 2013

Comparison of Control Approaches for Permanent Magnet Motors

EMIL KLINTBERG

Department of Energy and Environment
Division of Electric Power Engineering
CHALMERS UNIVERSITY OF TECHNOLOGY
Göteborg, Sweden 2013

Comparison of Control Approaches for Permanent Magnet Motors
EMIL KLINTBERG

Department of Energy and Environment
Division of Electric Power Engineering
Chalmers University of Technology
SE–412 96 Göteborg
Sweden
Telephone +46 (0)31–772 1000

Chalmers Bibliotek, Reproservice
Göteborg, Sweden 2013

Comparison of Control Approaches for Permanent Magnet Motors
EMIL KLINTBERG
Department of Energy and Environment
Division of Electric Power Engineering
Chalmers University of Technology

Abstract

This thesis deals with comparing control techniques for two existing permanent magnet motors with harmonics in their back emfs. To do so, ideal models of a Brushless DC (BLDC) motor and a Permanent Magnet Synchronous Motor (PMSM) have been modified to describe the behavior of two existing permanent magnet motors.

Comparisons of the motor constant and the relative torque ripple are performed when the motors are controlled with Field Oriented Control (FOC) as well as with traditional BLDC control.

A novel control scheme aiming at controlling the currents to have the same shape as the back emfs are presented. Simulations are performed to show how this method affects the motor constant and relative torque ripple.

Torque ripple due to phase commutation in BLDC motors is discussed and a version of lead angle adjustment is implemented to reduce this problem.

Even though an ideal BLDC motor has a higher motor constant than an ideal PMSM, simulations showed that a higher motor constant (almost 5% and about 2% for the two motors respectively) can be obtained by utilizing FOC compared to traditional BLDC control. A lower relative torque ripple (almost 86% and almost 44% for the two motors respectively) was also obtained for FOC compared to traditional BLDC control. A higher average torque per peak current was, however, obtained with traditional BLDC control. These results are valid for both motors.

Simulations showed that it is possible to achieve a higher motor constant, compared to FOC and traditional BLDC control, by controlling the currents to have the same shape as the back emfs. The relative torque ripple was however increased by using this method.

It is also shown, by an example, that the motor constant can be increased by implementing lead angle adjustment.

Index Terms: Permanent magnet motors, BLDC, PMSM, FOC, RLS, motor constant, torque ripple, phase commutation.

Acknowledgements

First and dearest I would like to thank my supervisor Prof. Torbjörn Thiringer for his supervision, friendly attitude and many good ideas. Regardless of his often high workload, he always makes time to answer questions as well as giving encouraging advice. You are highly appreciated!

I am also very grateful to Dr. Stefan Lundberg for lots of help in the laboratory, but also for good ideas and discussions regarding everything from implementations in Simulink to motors in general. What is said about Torbjörn is also true for you.

I would moreover like to thank Assoc. Prof. Massimo Bongiorno and PhD student Mebtu Beza for their patience, helpful attitude and sharing of their work regarding implementation of the RLS-algorithm.

Prof. Bo Egardt and Assoc. Prof. Torsten Wik are acknowledged for good discussions about issues regarding estimations in closed loop.

A thank also goes to Dr. Johan Åström for providing me with good simulation data for the BLDC motor.

I would also like to thank the whole department for a very friendly working environment, for letting me score every now and then when playing football and for making me feel very welcome during my thesis work.

Last, and certainly least, I would like to give a special thank to my brothers Anton Klintberg and Jacob Klintberg for supporting me, not only during this thesis work.

Emil Klintberg
Göteborg, Sweden, April 2013

Contents

Symbols and Glossary

Symbols and variables

b	Mechanical damping (Nms/rad)
e	Back emf (V)
f	Frequency (Hz)
I	Current amplitude (A)
i	Phase current (A)
J	Inertia (kgm^2)
j	Imaginary unit
K	Observer gain
k	Back emf shape (Vs/rad)
K_{ct}	Observer gain in continuous time
k_m	Motor constant ($Nm/W^{1/2}$)
L	Equivalent phase inductance (H)
L_s	Self inductance (H)
M	Mutual inductance (H)
n_p	Number of pole pairs
P	Covariance matrix
p	Differential operator
P_{loss}	Resistive losses in stator windings (W)
R	Phase resistance (Ω)
R_a	Active damping resistance (Ω)
t_{com}	Commutation time (s)
T_e	Electromechanical torque (Nm)
T_L	Load torque (Nm)
T_s	Sampling period (s)
t_{ri}	Rise time (s)
v	Phase-to-phase voltage (V)
V_d	DC-link voltage (V)
v_d	Diode voltage (V)
v_x	Phase voltage for phase x (V)
α_c	Bandwidth of current controller (rad/s)
α_{RLS}	Bandwidth of RLS (rad/s)
γ_{lead}	Tuning parameter

ΔT_e	Relative electromechanical torque ripple (Nm)
ε	Estimation error
θ	Vector of estimated parameters
θ_e	Electrical angle (rad)
θ_{lead}	Lead angle (rad)
θ_m	Mechanical angle (rad)
λ	Forgetting factor
ξ	Relative bandwidth
Ψ	Flux linkage (Wb)
ψ	Regression vector
ω_e	Electrical speed (rad/s)
ω_m	Mechanical speed (rad/s)

Superscripts

(dq)	dq-coordinates
$(\alpha\beta)$	$\alpha\beta$-coordinates

Subscripts

a, b, c	Phase quantities
d	d-component
q	q-component
ref	Reference
α	α-component
β	β-component

Abbreviations

BLDC	Brushless DC
emf	Electromotive Force
FOC	Field Oriented Control
IMC	Internal Model Control
PMSM	Permanent-Magnet Synchronous Motor
PWM	Pulse Width Modulation
RLS	Recursive Least Square
rpm	Revolutions Per Minute
SISO	Single Input Single Output

Chapter 1

Introduction

1.1 Background and motivation

Brushless DC (BLDC) motors were developed to offer a reliable, high performance and low maintenance alternative to DC-motors [1]. The basic principle of a BLDC motor is, however, the same as for a Permanent Magnet Synchronous Motor (PMSM), with the main difference that the BLDC motor does not need a sophisticated controller.

However, it has been shown that the control strategy for the BLDC motor is significant with aspect to the efficiency of the drive system, and that it in many cases can be beneficial to control a BLDC motor as a PMSM [2]. A thorough investigation of this can be found in [2]. It would therefore be interesting to investigate how the choice of control approach affects the performance of the motor in other ways.

This thesis will continue the comparison of control techniques for BLDC motors, by focusing on torque production. It will be investigated at which cost torque can be produced as well as the quality of the produced torque.

1.2 Aim and outline of this thesis

The purpose of this thesis is to investigate differences and issues regarding torque production for permanent magnet motors when different control techniques are utilized. The aim is moreover to quantify both the torque ability and the torque ripple for two existing BLDC motors when different control schemes are used.

Chapter 2 presents a brief background to permanent magnet motor drives. Basic principles of BLDC motors and PMSMs as well as basic operation of a frequency converter are presented.

Chapter 3 presents the models utilized in the rest of the work. It is also stated how the models of ideal motors can be modified to describe the behavior of real motors.

Chapter 4 introduces the real motors used in this work.

In Chapter 5 the current controllers are derived and presented.

Chapter 6 aims at quantifying the torque ability of the motors when different control techniques are utilized. To do so, the motor constant is used.

Chapter 7 quantifies the torque ripple in the simulations described in Chapter 6. A brief theoretical analysis of torque ripple due to phase commutation is also performed.

concluding remarks and suggestions for future work is given in Chapter 8.

Chapter 2

Permanent magnet motor drives

This chapter will give a brief background to permanent magnet motor drives. Basic principles of BLDC motors and PMSMs will be presented as well as basic operation of frequency converters.

2.1 Permanent magnet motors

All permanent magnet motors can be categorized as synchronous machines. However, depending on the shape of the supply voltage a further division is often made into BLDC motors, which are fed with trapezoidal voltages, and PMSMs which are fed with sinusoidal voltages.

This thesis will focus on a subset of these motors that are radially magnetized with surface mounted magnets.

2.1.1 Brushless DC motor

Firstly, it might seem strange that the BLDC motor is referred to as a DC-motor since it is evident that it is supplied with AC-voltage. Some clarity will however be given on this notation during the modeling of the motor, since the phase voltage equations ((3.4)-(3.6)) are identical to the armature voltage equation of a DC-motor. As a consequence, the BLDC motor is sometimes described as an inside-out DC-motor since it has its armature in the stator and magnets in the rotor [1].

A two pole BLDC motor is visualized in Figure 2.1. It is possible to observe that the rotor has permanent magnets creating two poles and that the stator consists of three phases evenly distributed over 60^o at each side of the stator.

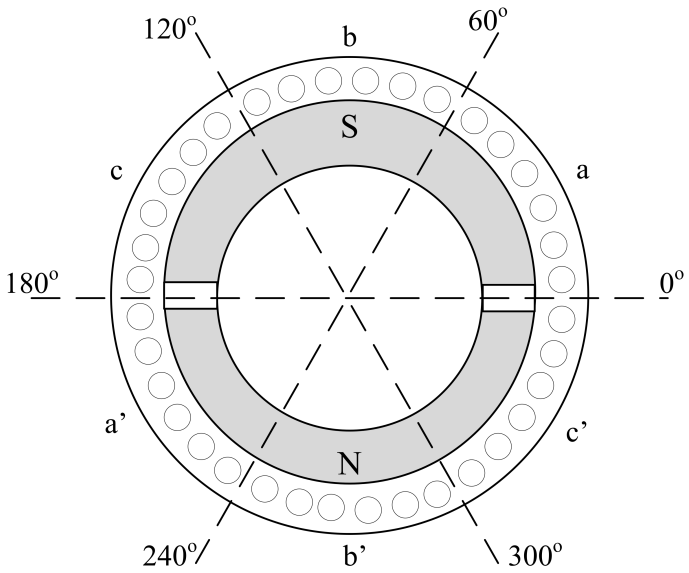

Fig. 2.1 Two pole BLDC motor

The ideal back emf in phase A, obtained by letting the motor in Figure 2.1 rotate counterclockwise, and the corresponding ideal current in phase A, to obtain a constant torque, are visualized in Figure 2.2(a) and Figure 2.2(b) respectively. The ideal back emfs and currents in the other phases have identical shapes as in phase A, but shifted 120^o towards each other and phase A.

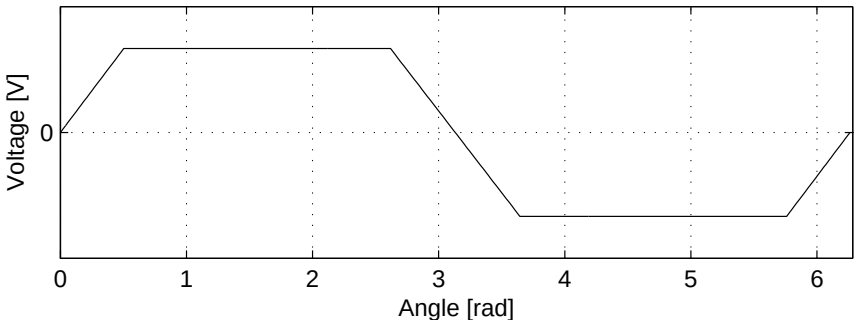

(a) e_a

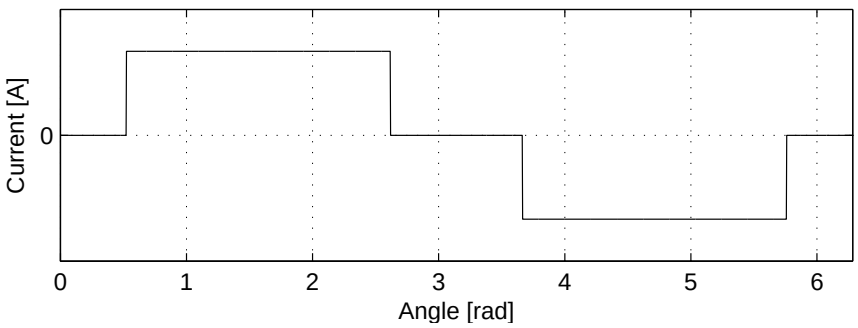

(b) i_a

Fig. 2.2 Ideal waveforms

Accordingly, the phases are excited to obtain currents that coincide with the flat parts

of the back emfs. Phase commutation is hence solely determined by rotor position, according to Figure 2.2(a)-2.2(b). From a control perspective it is hence sufficient to know the rotor angle at six positions for each electrical revolution, and the control can therefore be made very simple.

2.1.2 PMSM

A two pole PMSM is visualized in Figure 2.3 where it is possible to see that the stator windings, in contrast to the BLDC motor, in the ideal case are sinusoidally distributed [1]. Also the magnets on the rotor usually have a different shape compared to the BLDC motor, this is however not visible in Figure 2.3. As a result the induced back emfs are sinusoidal and the currents should also be sinusoidal to obtain a constant torque.

As a consequence, the control is more complex compared to the simple control of a BLDC motor. To be able to create sinusoidal currents with the same frequency and in phase with the back emfs, a synchronously rotating coordinate system aligned with the rotor flux linkage vector is often introduced. This system, often denoted as the dq-system, is visible in Figure 2.3 where it can be observed that the d-axis is aligned with the north pole of the magnet.

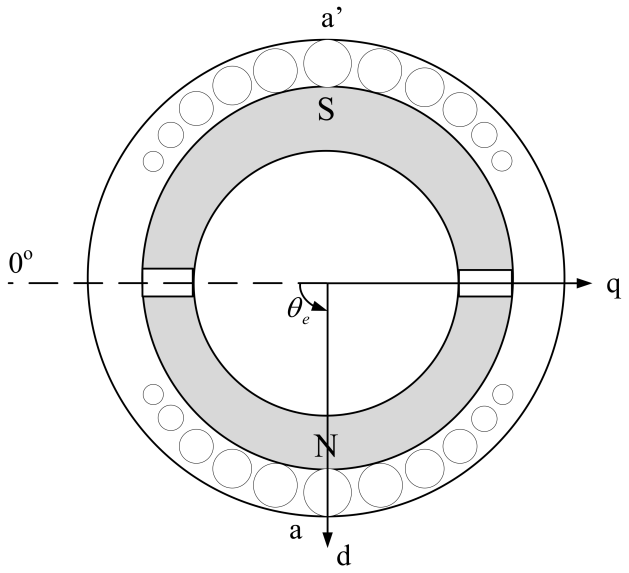

Fig. 2.3 Two pole PMSM. For clarity only the distribution of phase A is visualized.

2.2 Frequency converter

To be able to operate a permanent magnet motor, a frequency converter is needed. A circuit diagram of an often used frequency converter is visualized in Figure 2.4. The midpoint of the DC-link is used as ground and the points A, B and C can therefore have a potential of $\pm\frac{V_d}{2}$. Eight different switching states can hence be attained. A varying voltage with varying frequency can however be achieved in average by forming an intelligent

switching pattern (with several kHz) of these states [3]. This technique is denoted Pulse Width Modulation (PWM).

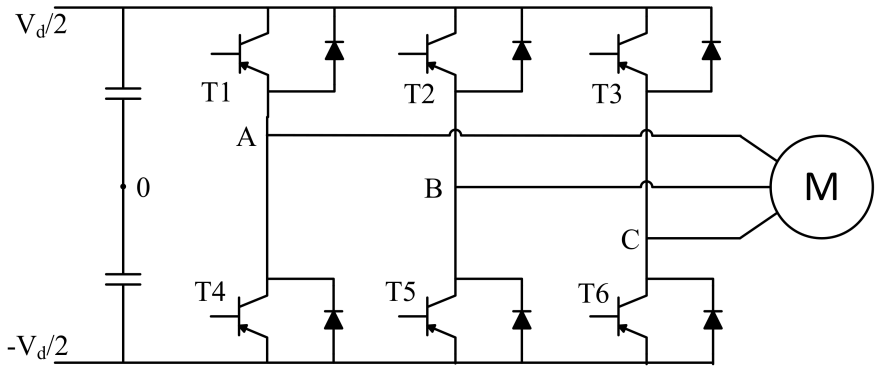

Fig. 2.4 Frequency converter

However, since this work focus on frequencies much lower than the switching frequency, it is assumed that the frequency converter can achieve an arbitrary voltage without using PWM. I.e. only the fundamental voltage component from the converter is considered and the harmonics are neglected.

Chapter 3

Modeling of permanent magnet motors

The aim of this chapter is to present the models utilized in the rest of the work. Derivations of models for an ideal BLDC motor and an ideal PMSM are presented. Furthermore, it is stated how the obtained models are modified to describe the behaviour of real motors.

The following assumptions are made in the modeling of the motors.

- The motors are unsaturated
- Eddy current and hysteresis effects do not affect the winding currents.
- The motors are nonsalient. Hence, the mutual and self inductances are constant and do not depend on rotor position.
- The frequency converters are constituted by ideal components.
- The phase resistance is independent of frequency.

3.1 Ideal Brushless DC motor

This section will present a derivation of the model utilized to describe an ideal BLDC motor. Both modeling of the motor itself and of six step operation are described.

3.1.1 Electrical modeling

By performing simple circuit observations, the following model of the BLDC motor (and three phase permanent magnet motors in general) can be obtained

$$v_a = Ri_a + L_s\frac{di_a}{dt} + M\frac{di_b}{dt} + M\frac{di_c}{dt} + e_a \tag{3.1}$$

$$v_b = Ri_b + M\frac{di_a}{dt} + L_s\frac{di_b}{dt} + M\frac{di_c}{dt} + e_b \tag{3.2}$$

$$v_c = Ri_c + M\frac{di_a}{dt} + M\frac{di_b}{dt} + L_s\frac{di_c}{dt} + e_c \tag{3.3}$$

where L_s and M represents the self and mutual inductance respectively, R represents the stator resistance and e_x the back emf in phase x. By assuming that there is no neutral wire

in the motor, the sum of the phase currents is zero and the model can be simplified to

$$v_a = Ri_a + (L_s - M)\frac{di_a}{dt} + e_a = Ri_a + L\frac{di_a}{dt} + e_a \tag{3.4}$$

$$v_b = Ri_b + (L_s - M)\frac{di_b}{dt} + e_b = Ri_b + L\frac{di_b}{dt} + e_b \tag{3.5}$$

$$v_c = Ri_c + (L_s - M)\frac{di_c}{dt} + e_c = Ri_c + L\frac{di_c}{dt} + e_c \tag{3.6}$$

where the equivalent phase inductance L has been introduced. Since the BLDC motor is controlled in a six step fashion where a controlled voltage is applied between two phases at the time, it is more convenient to have a model with the phase-to-phase voltages as inputs. A model of this type can be obtained by using (3.4) - (3.6) and that the sum of the phase currents is zero. A model is then obtained as

$$v_{ab} = R(i_a - i_b) + L\frac{d}{dt}(i_a - i_b) + e_{ab} \tag{3.7}$$

$$v_{bc} = R(i_b - i_c) + L\frac{d}{dt}(i_b - i_c) + e_{bc} \tag{3.8}$$

It is evident that only two equations are needed since the third would be a linear combination of the other two. To obtain a state space model, to implement in Simulink, (3.7) and (3.8) are modified to have only one current derivative in each equation. The model then becomes

$$\frac{di_a}{dt} = -\frac{R}{L}i_a + \frac{2}{3L}(v_{ab} - e_{ab}) + \frac{1}{3L}(v_{bc} - e_{bc}) \tag{3.9}$$

$$\frac{di_b}{dt} = -\frac{R}{L}i_b - \frac{1}{3L}(v_{ab} - e_{ab}) + \frac{1}{3L}(v_{bc} - e_{bc}) \tag{3.10}$$

and the last current is obtained from

$$i_c = -i_a - i_b \tag{3.11}$$

3.1.2 Mechanical modeling

For a three phase motor conservation of energy must apply in all phases simultaneously. By neglecting iron losses, this implies that the following holds

$$T_e\omega_m = e_a i_a + e_b i_b + e_c i_c \tag{3.12}$$

were ω_m and T_e represent mechanical speed and torque due to interaction between the magnetic field from the rotor and stator currents respectively. According to Faraday's law of induction a back emf can be written as

$$e_x = \frac{d\Psi_x}{dt} = \frac{d\Psi_x}{d\theta_e}\frac{d\theta_e}{dt} = k_x(\theta_e)\omega_e \tag{3.13}$$

where Ψ_x is the flux linkage and k_x is the speed independent shape of the back emf and will from here on be referred to as the *back emf shape*. By assuming that the back emfs in the three phases have the same shape and are separated by 120^o, it follow from (3.12) and (3.13) that

$$T_e = n_p(k(\theta_e)i_a + k(\theta_e - \frac{2\pi}{3})i_b + k(\theta_e - \frac{4\pi}{3})i_c) \tag{3.14}$$

where 'a' in k_a has been omitted to avoid cumbersome notations. The mechanical dynamics follows from Newton's law in rotating form.

$$J\frac{d\omega_m}{dt} = T_e - T_L - b\omega_m \tag{3.15}$$

where T_L and b represent a constant load torque and mechanical damping respectively. $T_L + b\omega_m$ can be regarded as a linearization of the load torque. Equation (3.14) and (3.15) can easily be implemented in Simulink to form a motor model together with the electrical equations (3.9) - (3.11).

3.1.3 Six step operation

It is not trivial to model six step operation in Simulink. This is due to difficulties to model the freewheeling diodes and hence to keep the current of the passive phase at zero. There are however different approaches to solve this problem [2], [4]. In this report, voltage sources are utilized to model the diodes.

By considering the diodes and transistors in Figure 2.4 to be ideal components, a simplified circuit can be drawn for each 60^o interval according to Figure 2.2(a)-2.2(b). This is visualized in Figure 3.1(a)-3.1(f).

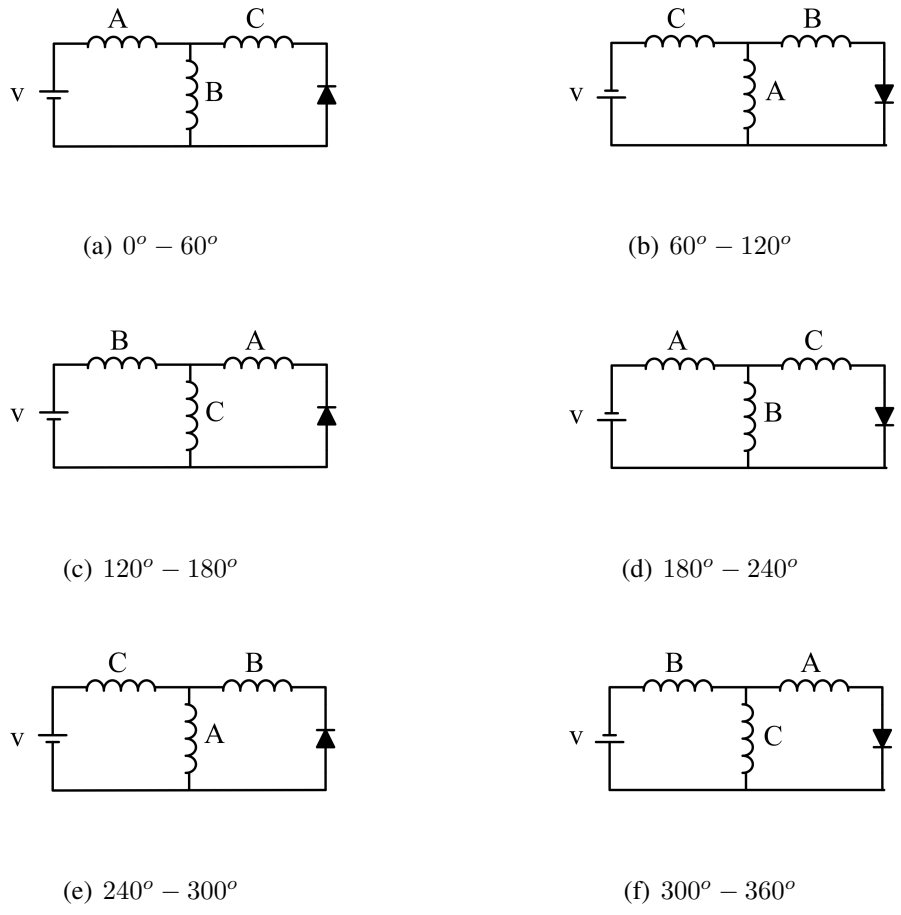

(a) $0^o - 60^o$

(b) $60^o - 120^o$

(c) $120^o - 180^o$

(d) $180^o - 240^o$

(e) $240^o - 300^o$

(f) $300^o - 360^o$

Fig. 3.1 Simplified circuits

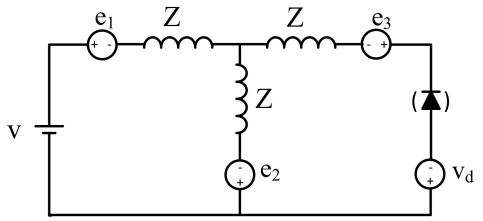

(a) Correspond to Figure 3.1(a), 3.1(c) and 3.1(e)

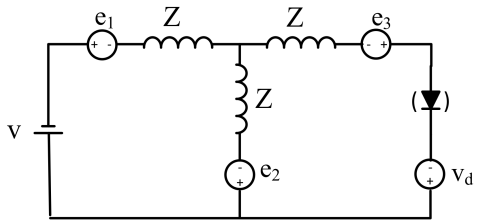

(b) Correspond to Figure 3.1(b), 3.1(d) and 3.1(f)

Fig. 3.2 Circuits illustrating diodes modeled with voltage sources

The idea is to replace the diodes with voltage sources acting as a diodes. That is to be zero when the diode is conducting and to have a voltage that prevents current to flow when the diode is not conducting. The voltage sources and circuits visualizing the principle are shown in Figure 3.2(a)-3.2(b). By performing circuit calculations to the circuits in Figure 3.2(a)-3.2(b) it is possible to find what voltage is needed to keep the current through the diode to be zero and then it is trivial to find the phase-to-phase voltages. The result, that is to be implemented in Simulink, is summarized in Table 3.1.

Table 3.1: Voltages to simulate six step operation

θ_e	Diode current	v_{ab}	v_{bc}	v_{ca}
$0^0 - 60^0$	$i_c \neq 0$	v	0	$-v$
	$i_c = 0$	v	$\frac{1}{2}(-v + e_a + e_b - 2e_c)$	$\frac{1}{2}(-v - e_a - e_b + 2e_c)$
$60^0 - 120^0$	$i_b \neq 0$	0	v	$-v$
	$i_b = 0$	$\frac{1}{2}(v + e_c + e_a - 2e_b)$	$\frac{1}{2}(v - e_c - e_a + 2e_b)$	$-v$
$120^0 - 180^0$	$i_a \neq 0$	$-v$	v	0
	$i_a = 0$	$\frac{1}{2}(-v - e_b - e_c + 2e_a)$	v	$\frac{1}{2}(-v + e_b + e_c - 2e_a)$
$180^0 - 240^0$	$i_c \neq 0$	$-v$	0	v
	$i_c = 0$	$-v$	$\frac{1}{2}(v + e_a + e_b - 2e_c)$	$\frac{1}{2}(v + e_a + e_b - 2e_c)$
$240^0 - 300^0$	$i_b \neq 0$	0	$-v$	v
	$i_b = 0$	$\frac{1}{2}(-v + e_c + e_a - 2e_b)$	$\frac{1}{2}(-v - e_c - e_a + 2e_b)$	v
$300^0 - 360^0$	$i_a \neq 0$	v	$-v$	0
	$i_a = 0$	$\frac{1}{2}(v - e_b - e_c + 2e_a)$	$-v$	$\frac{1}{2}(v + e_b + e_c - 2e_a)$

3.2 Ideal PMSM

This section will present a model of an ideal PMSM. The modeling of the PMSM is in principle the same as the modeling of the BLDC motor. However, since all three phases always are activated, it is beneficial to write the equations to be solved in another way. Hence, the classical two-axis representation is used.

3.2.1 Electrical modeling

The part of the stator voltage which is not dissipated in the stator resistance will contribute to building up a flux in the windings. Hence, the following expression must hold

$$v^{(\alpha\beta)} = Ri^{(\alpha\beta)} + \frac{d\Psi^{(\alpha\beta)}}{dt} \tag{3.16}$$

where $v^{(\alpha\beta)}$ represents stator voltage in $\alpha\beta$-coordinates, R represents stator resistance and $\Psi^{(\alpha\beta)}$ represents stator flux linkage in $\alpha\beta$-coordinates. The flux linking the stator coils are constituted of two parts, flux originated from the stator currents and flux originated from the permanent magnets in the rotor. This implies that the flux linkage can be expressed as

$$\Psi^{(\alpha\beta)} = Li^{(\alpha\beta)} + \Psi e^{j\theta_e} \tag{3.17}$$

where L is the stator inductance, $i^{(\alpha\beta)}$ is the stator current in $\alpha\beta$-coordinates and Ψ is the magnitude of the flux linkage from the rotor magnets. The flux linkage vector of the rotor rotates with the electrical speed and is displaced with the electrical angle from the α-axis. By using (3.17) in (3.16) the following state equation in $\alpha\beta$-coordinates, that is to be implemented in Simulink, is obtained

$$L\frac{di^{(\alpha\beta)}}{dt} = v^{(\alpha\beta)} - Ri^{(\alpha\beta)} - j\omega_e\Psi e^{j\theta_e} \tag{3.18}$$

where the term $j\omega_e\Psi e^{j\theta_e}$ from here on will be referred to as the back emf. For control purposes it is beneficial to transform (3.18) to dq-coordinates. The following is then obtained

$$L\frac{di^{(dq)}}{dt} = v^{(dq)} - Ri^{(dq)} - j\omega_e Li^{(dq)} - j\omega_e\Psi e^{j(\theta-\theta_e)} \tag{3.19}$$

where the term $j\omega_e Li^{(dq)}$ from here on will be referred to as the cross coupling term and $j\omega_e\Psi e^{j(\theta-\theta_e)}$ will be referred to as back emf.

3.2.2 Mechanical modeling

Just as for the BLDC motor conservation of energy must apply in all phases simultaneously. This implies that the following holds (for amplitude invariant transformation)

$$T_e\omega_m = -\frac{3}{2}Re(j\omega_e\Psi e^{j\theta_e}i^{(\alpha\beta)}) \tag{3.20}$$

The minus sign is needed since the stator currents and the back emfs are not defined in the same direction. From (3.20) it is now possible to find the torque as

$$T_e = \frac{3n_p}{2}\Psi(\cos\theta_e i_\beta - \sin\theta_e i_\alpha) \tag{3.21}$$

The mechanical dynamics is also in this case determined by (3.15).

3.3 Modeling of real permanent magnet motors

To obtain models for non ideal motors only minor modifications of the described models are needed. The model of the BLDC motor is changed by replacing the back emfs in (3.9) and (3.10) as well as replacing the back emf shape in (3.14). The same modifications can be done in the model of the PMSM by changing the back emf in (3.18) and the back emf shape in (3.20). Obviously, the modifications can be obtained by including a non ideal back emf shape in the models. The back emf shapes for the motors, that will be introduced in the next chapter, are visualized in Figure 3.3(a) and Figure 3.3(b).

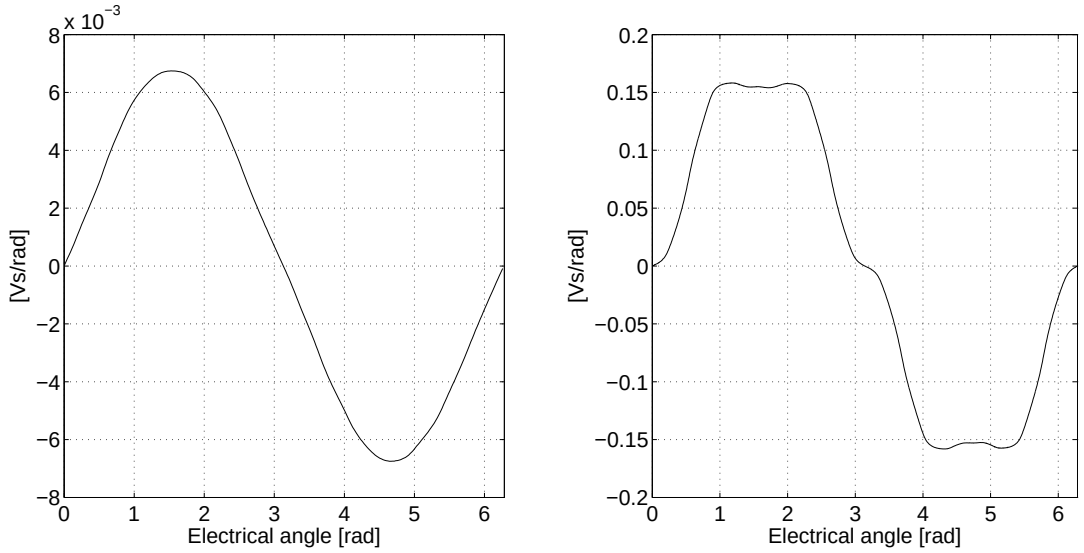

(a) Airplane motor (b) BLDC motor

Fig. 3.3 Back emf shapes

ï»¿

Chapter 4

Parameters and waveforms from real permanent magnet motors

The simulation models described in Chapter 3 are going to be adapted to two different BLDC motors. One that has a low amount of harmonics in the back emf and therefore is close to a PMSM, and one that has a harmonic content in the back emf which makes it more similar to an ideal BLDC motor.

4.1 Airplane motor

The motor that is going to be referred to as the *Airplane motor* is a low voltage and high speed BLDC motor, typically used in radio controlled model airplanes. The motor was originally connected in delta, but was reconnected to Y to eliminate losses due to circulating currents in the delta. The available information about this motor is however very limited and therefore motor parameters, needed for model building, had to be determined by experiments. The obtained parameters are summarized in Table 4.1 and the back emfs and an amplitude spectrum of the back emfs are visualized in Figure 4.1(a) and Figure 4.1(b) respectively.

Table 4.1: Motor parameters for the Airplane motor

Connection	Y	
No. of pole pairs	n_p	10
Resistance (f = 0 Hz)	R	6.5 $m\Omega$
Self inductance	L_s	12.3 μH
Mutual inductance	M	0.7 μH
Permanent magnet flux linkage	Ψ	6.74 mWb
Inertia	J	2.13 $mkgm^2$
Damping	b	4.45 $mNms/rad$

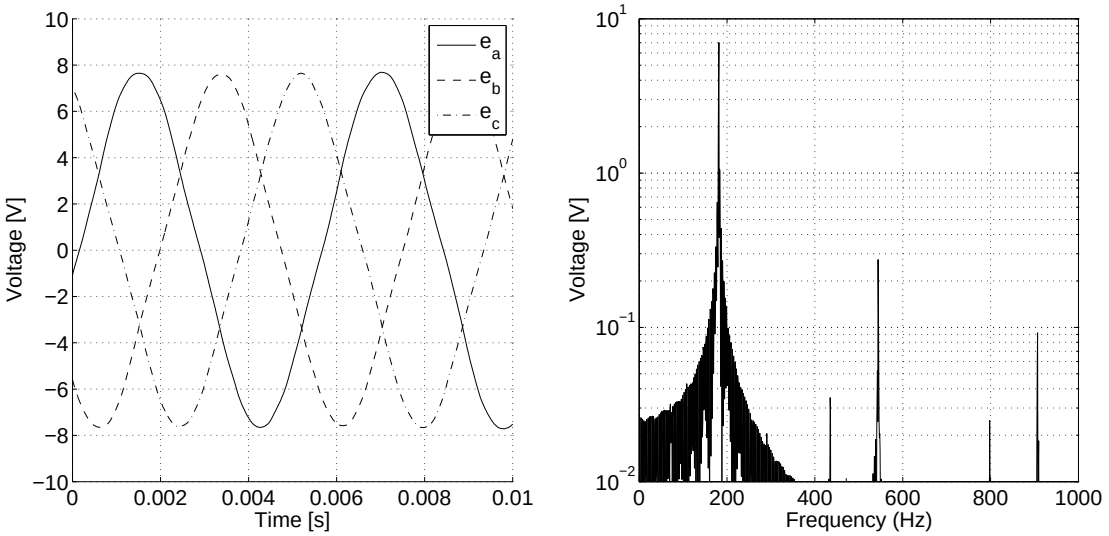

(a) Back emfs (b) FFT of back emf

Fig. 4.1 Airplane motor at 1083 rpm

4.2 BLDC motor

The motor that is going to be referred to as the *BLDC motor*, is a BLDC motor designed by J. Åström and is intended for fan applications. The electrical motor parameters and waveforms that are used are obtained from simulations in Maxwell/Simplorer. The mechanical parameters are roughly estimated from the geometry of the motor. Deviations in the mechanical parameters will however not influence the result of this work. The parameters are summarized in Table 4.2 and the back emfs and an amplitude spectrum of the back emfs are visualized in Figure 4.2(a) and Figure 4.2(b) respectively.

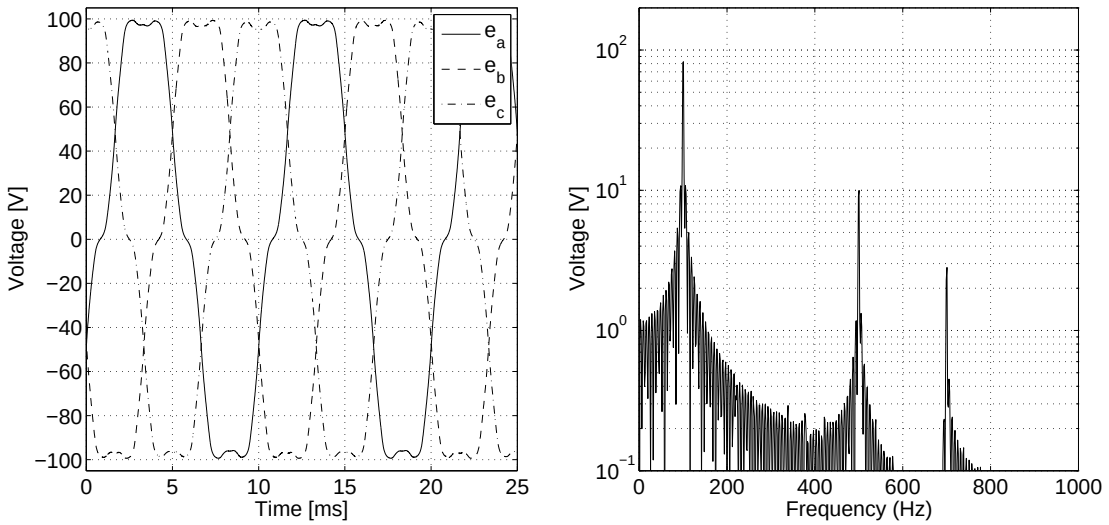

(a) Back emfs (b) FFT of back emf

Fig. 4.2 BLDC motor at 1000 rpm

Table 4.2: Motor parameters for the BLDC motor

Connection	Y	
No. of pole pairs	n_p	6
Resistance (f = 0 Hz)	R	0.65 Ω
Self inductance	L_s	5.4 mH
Mutual inductance	M	2.7 mH
Permanent magnet flux linkage	Ψ	168 mWb
Inertia	J	1.67 $mkgm^2$
Damping	b	60 $mNms/rad$

Chapter 5

Current control

This chapter will present the controllers used in this work. A standard vector control scheme is presented, here denoted as Field Oriented Control (FOC). The field oriented control is then modified to also utilize field oriented control of the harmonics. Furthermore, a traditional BLDC control scheme as well as a modified version of traditional BLDC control are described.

5.1 Field oriented control

When designing the current controller it is assumed that the electrical dynamics are much faster than the mechanical dynamics. This implies that ω_e can be regarded to be constant during the design. Moreover, (3.19) is visualized as a block diagram in Figure 5.1, where the cross coupling term is visualized as a feedback term and the back emf as a load disturbance. The block $G^{'}(p)$ then becomes a complex valued transfer function without any coupling between the real and imaginary parts.

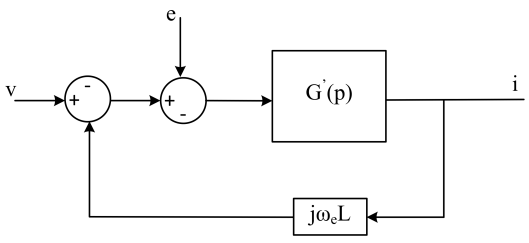

Fig. 5.1 Block diagram of electrical dynamics

It can be realized from Figure 5.1, that the motor is described by two Single-Input Single-Output (SISO) systems with a coupling in between. This coupling can however be compensated for, and two non coupled SISO systems are then obtained.

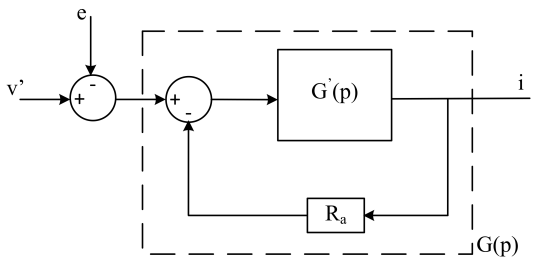

Fig. 5.2 Block diagram with active damping

The design approach that is going to be utilized is Internal Model Control (IMC), and an inherent drawback with this method is poor response from a load disturbance [5]. The response can however be improved by adding active damping [6]. That is to add extra resistance to the model by introducing an inner feedback loop, as visualized in Figure 5.2. To further reduce this effect, feed forward of back emf is also implemented. To sum up, (3.19) is reduced to

$$L\frac{di^{(dq)}}{dt} = v'^{(dq)} - (R + R_a)i^{(dq)} \tag{5.1}$$

by choosing

$$v^{(dq)} = v'^{(dq)} - (R_a - j\omega_e\hat{L})i^{(dq)} + j\omega_e\hat{\Psi} \tag{5.2}$$

A block scheme of field oriented control is visualized in Figure 5.3.

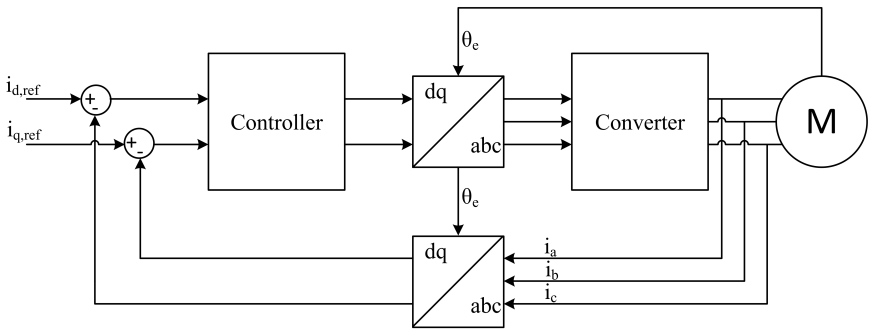

Fig. 5.3 Block scheme of field oriented control.

5.1.1 Design of IMC controller

If the system that is to be controlled is perfectly known, stable and well damped and there are no disturbances, feedback would not be needed. The idea of IMC is then to only use feedback for information originated from model errors, disturbances and other *new information* [5]. A typical block scheme illustrating this principle is shown in Figure 5.4.

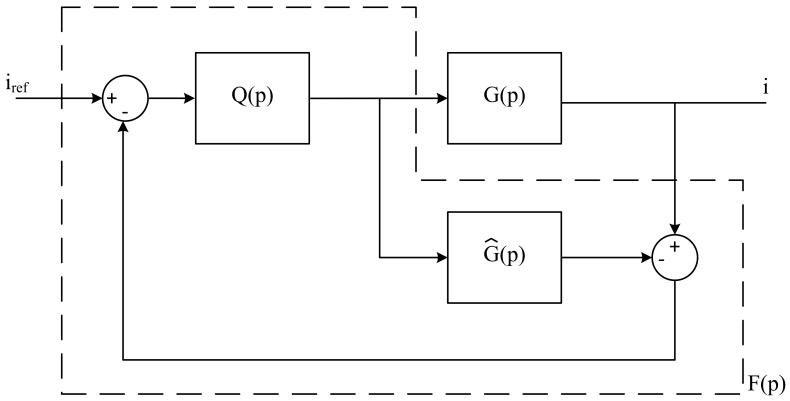

Fig. 5.4 Block scheme illustrating IMC

The design is then a question of choosing $Q(p)$. A common choice is

$$Q(p) = (\frac{\alpha_c}{p+\alpha_c})^n \hat{G}^{-1}(p) \tag{5.3}$$

where n is chosen to make $Q(p)$ realizable [5] and $\hat{G}(p)$ is a model of the system. Notice that for no model errors, this will make the closed loop system to be

$$G_c(p) = (\frac{\alpha_c}{p+\alpha_c})^n \tag{5.4}$$

and α_c is hence the bandwidth of the closed loop system for $n = 1$. Since the system to be controlled is of first order, $n = 1$ is sufficient. It is then also straight forward to show that this choice make the controller $F(p)$, which is visualized in Figure 5.4, to be an ordinary PI controller according to

$$F(p) = \frac{\alpha_c}{p}\hat{G}^{-1}(p) = \alpha_c\hat{L} + \frac{\alpha_c(\hat{R}+R_a)}{p} \tag{5.5}$$

If the inner feedback loop is chosen to be as fast as the closed loop system, this implies that R_a should be chosen as

$$R_a = \alpha_c\hat{L} - \hat{R} \tag{5.6}$$

By using (5.6) in (5.5) the controller can be found to be

$$F(p) = \alpha_c\hat{L} + \frac{\alpha_c^2\hat{L}}{p} = k_p + \frac{k_i}{p} \tag{5.7}$$

5.1.2 Evaluation of current controller

To evaluate the performance of the current controller, a step response is simulated. The simulation is performed with the model of the ideal PMSM, adopted with the parameters from the Airplane motor. The bandwidth of the current controller is chosen to be $\alpha_c = 1000\ rad/s$ and the result is visualized in Figure 5.5(a)-5.5(b). Observe that the $10\% - 90\%$ rise time t_{ri} can be calculated from the following well known expression for a first order system to

$$t_{ri} = \frac{\ln 9}{\alpha_c} \approx 2.2\,ms \tag{5.8}$$

which correspond well with the behavior of i_q in Figure 5.5(a).

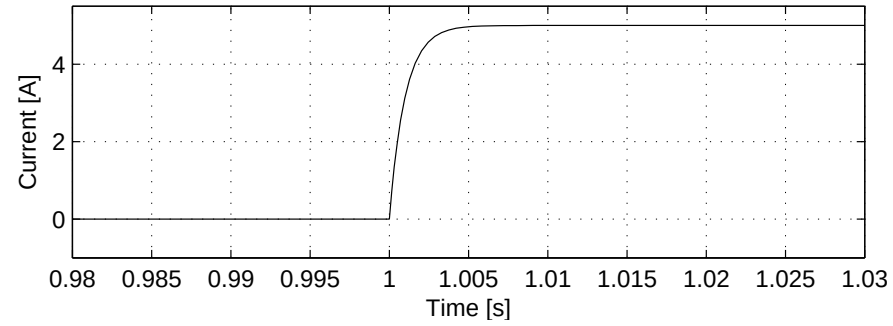

(a) i_q

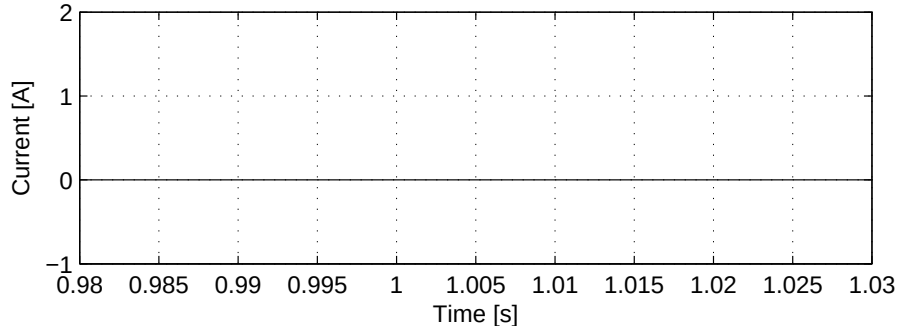

(b) i_d

Fig. 5.5 Step response. A step in the quadrature current reference to 5 A is performed at 1 s.

5.2 Field oriented control of harmonics

To obtain the highest possible torque per RMS-current ratio, the currents should be controlled to have the same harmonic content as the back emfs, provided that the currents and back emfs are in phase [2]. To achieve this, the FOC approach will be modified by introducing a controller for each of the most significant harmonic components in the back emfs as well as a Recursive Least Square (RLS) algorithm to find the harmonics in the current. This is visualized as a block scheme in Figure 5.6. The RLS algorithm is described in detail in Section 5.2.2.

This approach will only be implemented for the BLDC motor and not for the Airplane motor, since the harmonic content in the back emfs of the latter is too low.

It can be observed in Figure 4.2(b) that the back emfs of the BLDC motor to a large extent are composed by a fundamental, a 5^{th} and a 7^{th} harmonic. It is therefore desirable to find these components in the current and control them to coincide with their corresponding components in the back emf. The current references for the 5^{th} and 7^{th} harmonic are hence chosen to obtain the same ratio between the components as in the back emf. Hence, for the BLDC motor the references are chosen according to

$$i_{5,ref}^{(dq)} = 0.1209 i_{ref}^{(dq)} \tag{5.9}$$

$$i_{7,ref}^{(dq)} = -0.03408 i_{ref}^{(dq)} \tag{5.10}$$

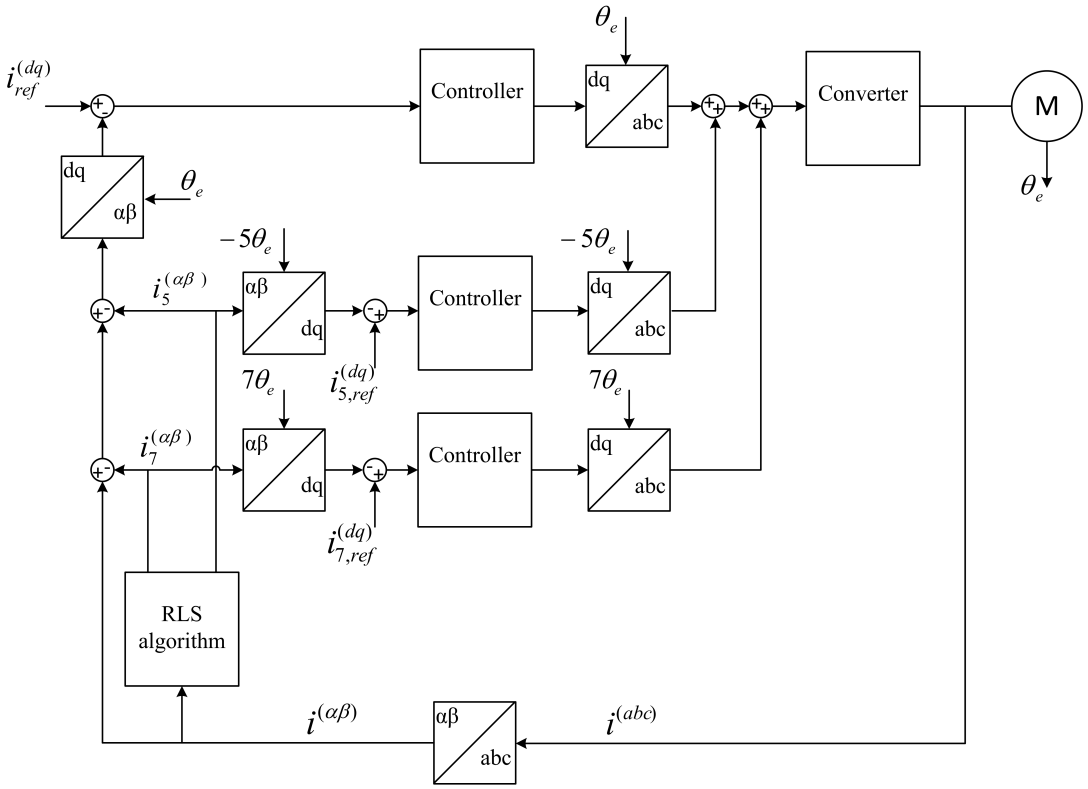

Fig. 5.6 Modified field oriented control.

5.2.1 Evaluation of field oriented control of harmonics

To evaluate the performance of the controller, a step response is simulated. The model of the BLDC motor is used for the simulation and the bandwidth of the controller for the fundamental current component is chosen to be $\alpha_c = 1000\ rad/s$. The bandwidth of the RLS and the bandwidths of the controllers for the harmonics are however varied with the speed of the machine according to

$$\alpha_{RLS} = \alpha_{c,5} = \alpha_{c,7} = 4\omega_e \tag{5.11}$$

The settings utilized in the simulation are summarized in Table 5.1.

Table 5.1: Simulation settings

Step time	$1\ s$
$i_{q,ref}$	$5\ A$
$i_{q5,ref}$	$0.6045\ A$
$i_{q7,ref}$	$-0.1704\ A$

The response for the q- and d-part of the fundamental current component are visualized in Figure 5.7(a) and Figure 5.7(b) respectively. The 5^{th} current harmonic is visualized in Figure 5.8(a)-5.8(b) and the 7^{th} current harmonic is visualized in Figure 5.9(a)-5.9(b). The phase currents are visualized in Figure 5.10(a)-5.10(c), and the currents in steady state are visualized in Figure 5.11(a)-5.11(c). Observe that the steady state currents in Figure

5.11(a)-5.11(c) have a very similar shape as the back emfs visualized in Figure 4.2(a). The convergence of the RLS is visualized in Figure 5.12(a)-5.12(a) where the estimated currents are depicted with the real currents.

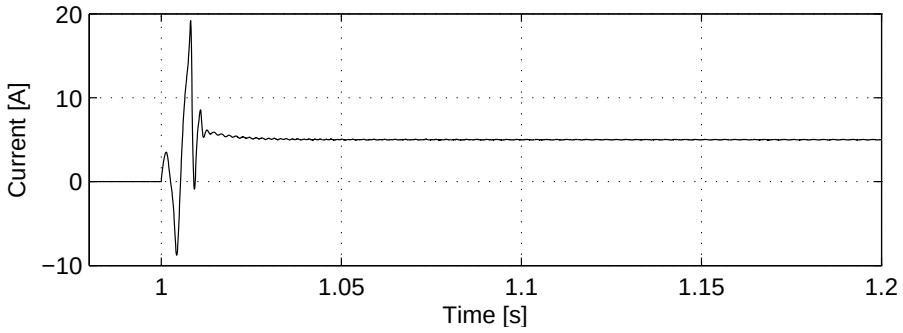

(a) i_{q1}

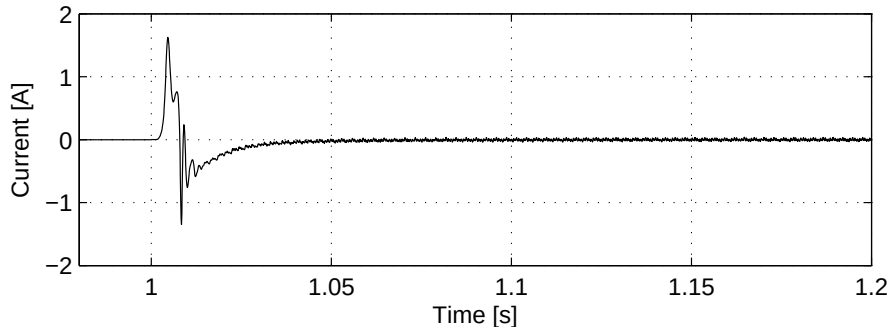

(b) i_{d1}

Fig. 5.7 Fundamental current component during a step response

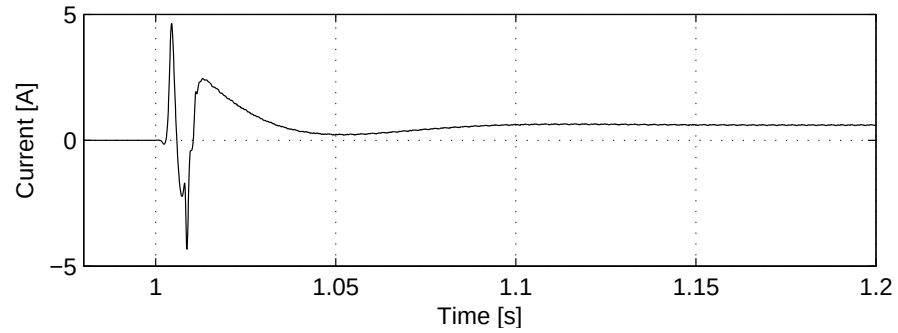

(a) i_{q5}

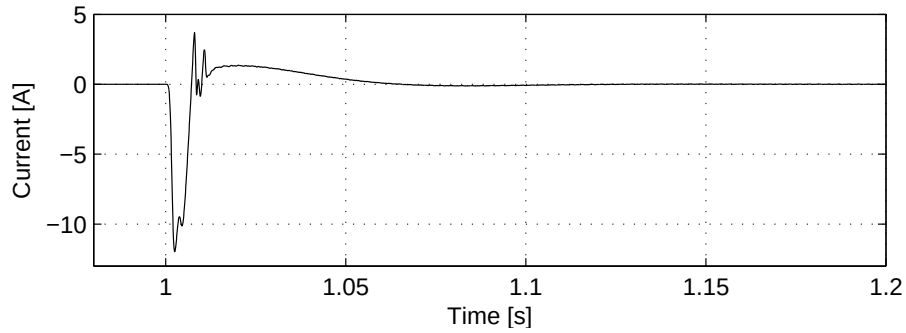

(b) i_{d5}

Fig. 5.8 5^{th} current harmonic during a step response

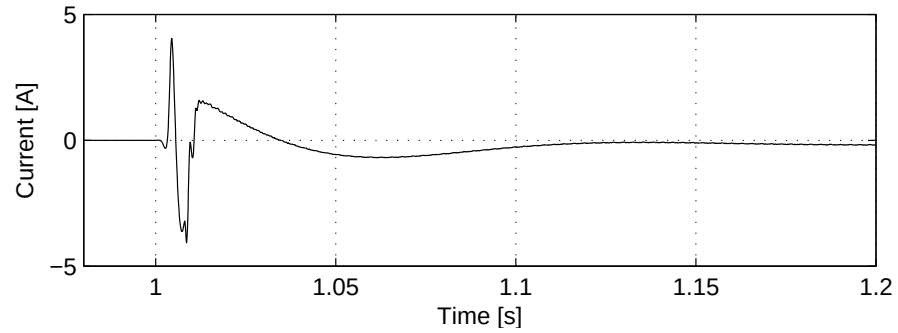

(a) i_{q7}

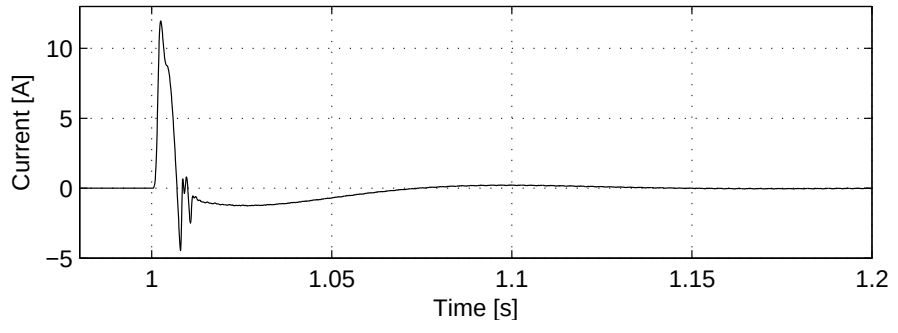

(b) i_{d1}

Fig. 5.9 7^{th} current harmonic during a step response

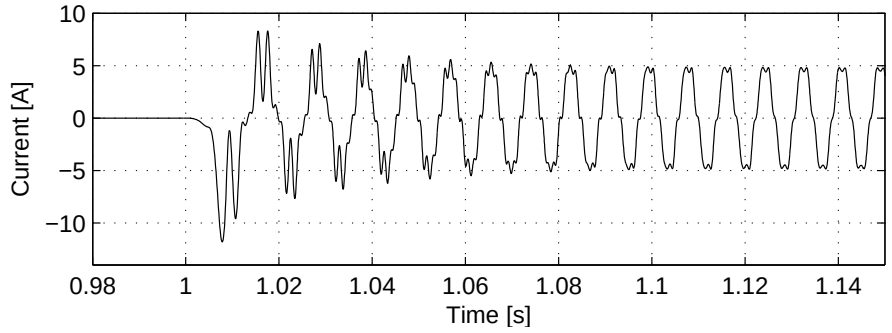

(a) i_a

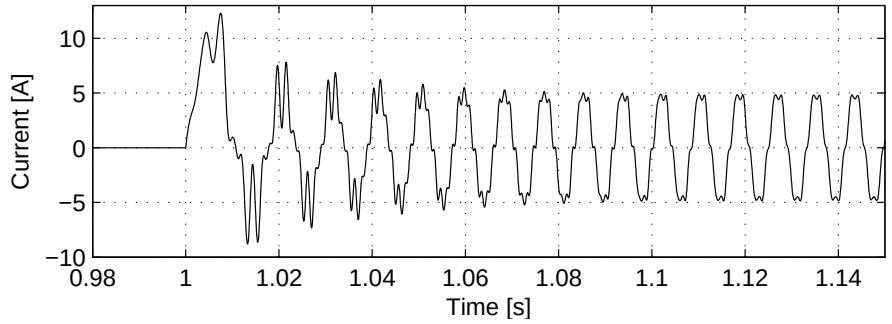

(b) i_b

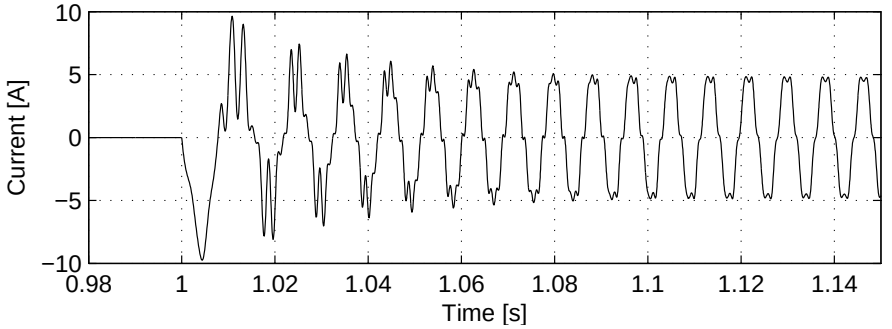

(c) i_c

Fig. 5.10 Phase currents during a step response

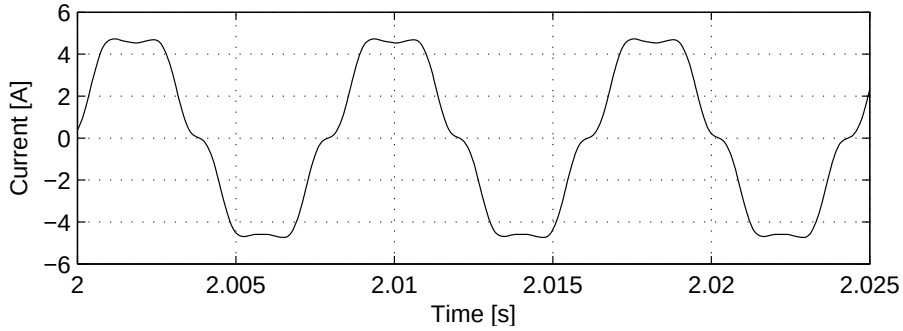

(a) i_a

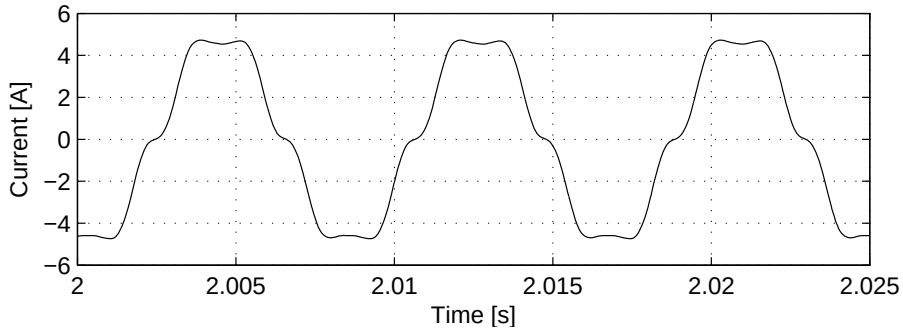

(b) i_b

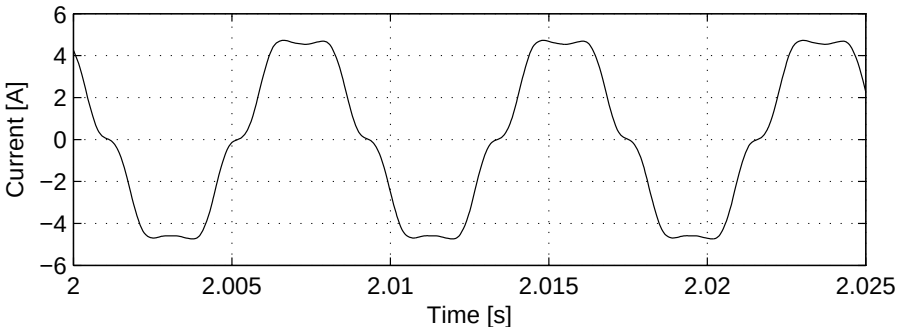

(c) i_c

Fig. 5.11 Phase currents in steady state

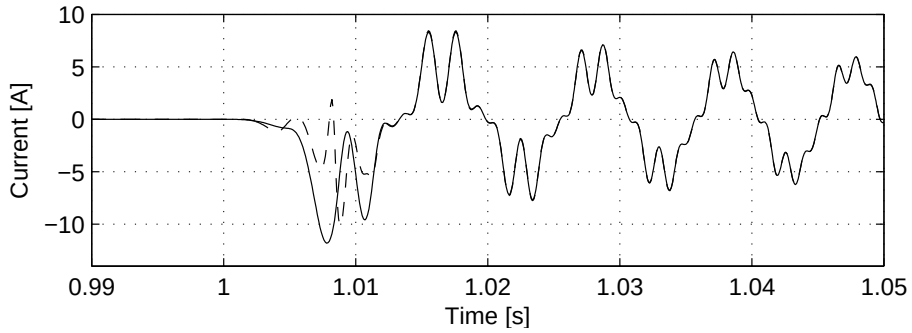

(a) i_α solid. $\hat{i}_\alpha$ dashed.

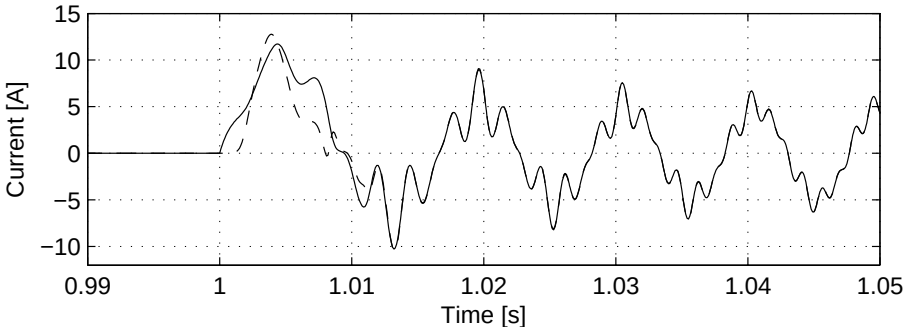

(b) i_β solid. $\hat{i}_\beta$ dashed.

Fig. 5.12 Estimated and real current

5.2.2 Estimation of harmonic content with Recursive Least Square

When slow estimations are acceptable, it has been shown that RLS algorithms has a similar dynamic performance as low pass filter based approaches [7], [8]. However, when fast estimations are needed, the dynamic performance of RLS based approaches are often superior to approaches based on low pass filters. This is for instance described in an application similar to this one in [8]. The RLS algorithm minimizes the following sum of squared estimating errors

$$J(\theta) = \frac{1}{2}\sum_{k=1}^{t} \lambda^{t-k}\varepsilon^2(k) \tag{5.12}$$

where ε represent the estimation error and λ is the so called *forgetting factor* which is introduced to handle time varying quantities. The algorithm obtained from minimizing (5.12) is as follows

$$\hat{\theta}(t) = \hat{\theta}(t-1) + K(t)\varepsilon(t) \tag{5.13}$$

$$\varepsilon(t) = y(t) - \psi^T(t)\hat{\theta}(t-1) \tag{5.14}$$

$$K(t) = P(t)\psi(t) = \frac{P(t-1)\psi(t)}{\lambda I + \psi^T P(t-1)\psi(t)} \tag{5.15}$$

$$P(t) = \frac{1}{\lambda}(P(t-1) - \frac{P(t-1)\psi(t)\psi^T(t)P(t-1)}{\lambda I + \psi^T P(t-1)\psi(t)}) = \frac{1}{\lambda}(I - K(t)\psi^T(t))P(t-1) \tag{5.16}$$

where K and P represent the *observer gain* and *covariance matrix* respectively, $\hat{\theta}$ is a vector containing estimated parameters and ψ is the so called *regression vector* which contain known functions in which the parameters are linear.

Recall that the back emfs of the BLDC motor to a large extent are composed of a fundamental, a 5^{th} and a 7^{th} harmonic. By neglecting higher order harmonics, the current can then be expressed as

$$i^{(\alpha\beta)} = I_1^{(\alpha\beta)} e^{j\theta_e} + I_5^{(\alpha\beta)} e^{-j5\theta_e} + I_7^{(\alpha\beta)} e^{j7\theta_e} \tag{5.17}$$

where $I_1^{(\alpha\beta)}$, $I_5^{(\alpha\beta)}$ and $I_7^{(\alpha\beta)}$ are the complex amplitudes that are going to be estimated. By expanding (5.17) and separating the real and imaginary parts, the following vectors in the RLS-algorithm can be identified.

$$\hat{\theta}^T = \begin{bmatrix} \hat{I}_{1\alpha} & \hat{I}_{1\beta} & \hat{I}_{5\alpha} & \hat{I}_{5\beta} & \hat{I}_{7\alpha} & \hat{I}_{7\beta} \end{bmatrix} \tag{5.18}$$

$$\psi^T = \begin{bmatrix} \cos(\theta_e) & -\sin(\theta_e) & \cos(5\theta_e) & \sin(5\theta_e) & \cos(7\theta_e) & -\sin(7\theta_e) \\ \sin(\theta_e) & \cos(\theta_e) & -\sin(5\theta_e) & \cos(5\theta_e) & \sin(7\theta_e) & \cos(7\theta_e) \end{bmatrix} \tag{5.19}$$

$$y^T = \begin{bmatrix} i_\alpha & i_\beta \end{bmatrix} \tag{5.20}$$

Steady-state model of the RLS algoritm

To avoid very cumbersome calculations during this analysis, the sizes of the matrices are reduced by allowing the RLS to be complex valued. Notice however that the RLS algorithm is exactly the same as previously stated, only slightly different notations are used. By allowing complex values the following vectors can be identified

$$\hat{\theta}^T = \begin{bmatrix} \hat{I}_1^{(\alpha\beta)} & \hat{I}_5^{(\alpha\beta)} & \hat{I}_7^{(\alpha\beta)} \end{bmatrix} \tag{5.21}$$

$$\psi^T = \begin{bmatrix} e^{j\omega_e t} & e^{-j5\omega_e t} & e^{j7\omega_e t} \end{bmatrix} \tag{5.22}$$

$$y = i_\alpha + j i_\beta \tag{5.23}$$

By assuming that the sampling period T_s is small the following can be obtained from (5.13)

$$\frac{\hat{\theta}(kT_s) - \hat{\theta}((k-1)T_s)}{T_s} \approx \frac{d\hat{\theta}}{dt} = K_{ct}(t)(y(t) - \psi^T(t)\hat{\theta}(t)) \tag{5.24}$$

where a new observer gain K_{ct} has been defined as

$$K_{ct} = \frac{K}{T_s} \tag{5.25}$$

Moreover, note that $\hat{\theta}$ contains estimates of amplitudes, while y and ψ contain periodic functions. By realizing this, two important observations can be made.

- It is not possible to find transfer functions from y to the estimated parameters in $\hat{\theta}$.
- The observer gain K_{ct} is time varying.

To be able to analyse the steady state behavior of the filter in a convenient way and find transfer functions from y to the parameters in $\hat{\theta}$, the following new parameters are introduced

$$i_1^{(\alpha\beta)} = I_1^{(\alpha\beta)} e^{j\omega_e t} \tag{5.26}$$
$$i_5^{(\alpha\beta)} = I_5^{(\alpha\beta)} e^{-j5\omega_e t} \tag{5.27}$$
$$i_7^{(\alpha\beta)} = I_7^{(\alpha\beta)} e^{j7\omega_e t} \tag{5.28}$$

By using (5.26)-(5.28) in (5.24), the following state space representation can be obtained

$$\begin{aligned}\frac{d}{dt}\begin{bmatrix} i_1^{(\alpha\beta)} \\ i_5^{(\alpha\beta)} \\ i_7^{(\alpha\beta)} \end{bmatrix} \\ = \begin{bmatrix} -K_{ct}(1)e^{j\omega_e t} + j\omega_e & -K_{ct}(1)e^{j\omega_e t} & -K_{ct}(1)e^{j\omega_e t} \\ -K_{ct}(2)e^{-j5\omega_e t} & -K_{ct}(2)e^{-j5\omega_e t} - j5\omega_e & -K_{ct}(2)e^{-j5\omega_e t} \\ -K_{ct}(3)e^{j7\omega_e t} & -K_{ct}(3)e^{j7\omega_e t} & -K_{ct}(3)e^{j7\omega_e t} + j7\omega_e \end{bmatrix} \begin{bmatrix} i_1^{(\alpha\beta)} \\ i_5^{(\alpha\beta)} \\ i_7^{(\alpha\beta)} \end{bmatrix} \\ + \begin{bmatrix} K_{ct}(1)e^{j\omega_e t} \\ K_{ct}(2)e^{-j5\omega_e t} \\ K_c(3)e^{j7\omega_e t} \end{bmatrix} y(t)\end{aligned} \tag{5.29}$$

where $K_{ct}(n)$ represent the n^{th} element in the observer gain vector K_{ct}. A steady state model can thus be found, by finding the observer gain in steady state. The inverse of the covariance matrix in continuous time is given by [9]

$$P^{-1}(t) = \int_0^t e^{-\alpha_{RLS}(t-\tau)} \psi(\tau)\psi^T(\tau) d\tau \tag{5.30}$$

where the steady state bandwidth of the RLS is given by [10]

$$\alpha_{RLS} = \frac{1-\lambda}{T_s} \tag{5.31}$$

By using (5.30), the observer gain can then be found from (5.15) and hence the coefficients in the state space model. The obtained state space model is as follows

$$\frac{d}{dt}\begin{bmatrix} i_1^{(\alpha\beta)} \\ i_5^{(\alpha\beta)} \\ i_7^{(\alpha\beta)} \end{bmatrix} = \begin{bmatrix} -\kappa_1 + j\omega_e & -\kappa_1 & -\kappa_1 \\ -\kappa_5 & -\kappa_5 - j5\omega_e & -\kappa_5 \\ -\kappa_7 & -\kappa_7 & -\kappa_7 + j7\omega_e \end{bmatrix} \begin{bmatrix} i_1^{(\alpha\beta)} \\ i_5^{(\alpha\beta)} \\ i_7^{(\alpha\beta)} \end{bmatrix} + \begin{bmatrix} \kappa_1 \\ \kappa_5 \\ \kappa_7 \end{bmatrix} y(t) \tag{5.32}$$

where the relative bandwidth is defined as

$$\xi = \frac{\alpha_{RLS}}{\omega_e} \tag{5.33}$$

and the coefficients in the state space are defined as

$$\kappa_1 = \alpha_{RLS}\left(\frac{1}{36}\xi^2 + \frac{2}{3} + j\left(\frac{1}{6}\xi + \frac{16}{9\xi}\right)\right) \tag{5.34}$$

$$\kappa_5 = \alpha_{RLS}\left(\frac{-1}{72}\xi^2 + \frac{1}{6} + j\left(\frac{1}{6}\xi + \frac{10}{9\xi}\right)\right) \tag{5.35}$$

$$\kappa_7 = \alpha_{RLS}\left(\frac{-1}{72}\xi^2 + \frac{7}{9} + j\left(\frac{7}{36}\xi + \frac{8}{9\xi}\right)\right) \tag{5.36}$$

Steady-state analysis of the RLS algoritm

The forgetting factor λ is a measure of the speed at which old data are forgotten, and hence a design variable regarding the speed of the estimation. The choice of the forgetting factor, and hence the bandwidth of the RLS, is therefore a tradeoff between speed of response and frequency selectivity. A high bandwidth implies fast response and a low bandwidth implies high selectivity. To evaluate the frequency selectivity, frequency responses from the measured current to the estimated current components are studied. To obtain a similar behavior for all motor speeds, simulations have shown that a good performance is obtained by keeping the relative bandwidth constant. Frequency responses for two different speeds are visualized in Figure 5.13(a)-5.13(f) and Figure 5.14(a)-5.14(f). Observe that the filter has unit gain and no phase shift for the estimated frequency component, and acts as notch filters for the other components.

It is also important to notice that, even though the complexity of the system increases by varying the bandwidth of the RLS, it has some benefits. If the regression vector is constant for some time it results in wind up in the covariance matrix [9], i.e. the entries grow exponentially with λ. Note however that this is prevented by keeping the relative bandwidth constant, since this gives $\lambda = 1$ at $\omega_e = 0$.

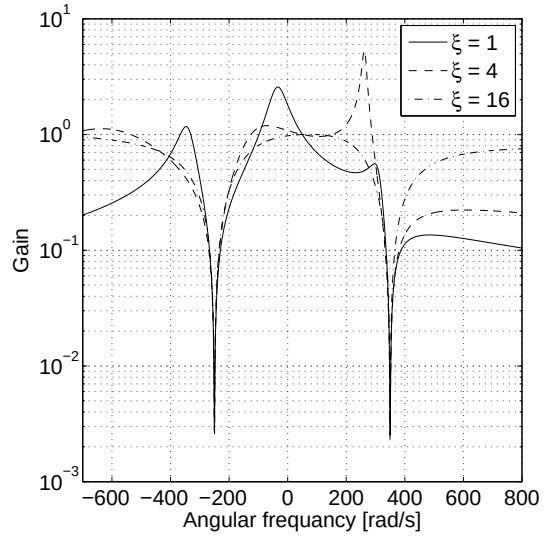

(a) Amplitude of frequency response from $i^{(\alpha\beta)}$ to $i_1^{(\alpha\beta)}$

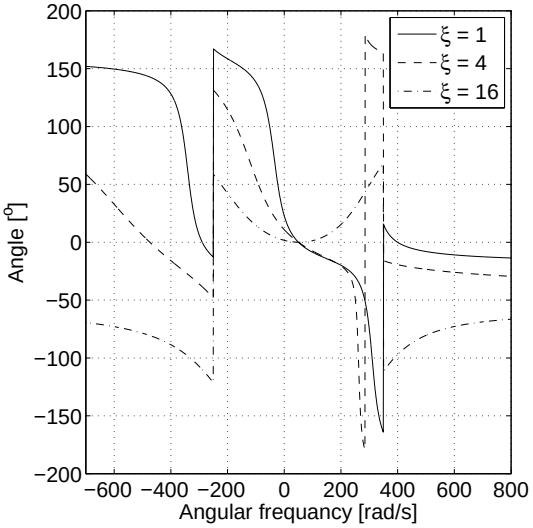

(b) Phase of frequency response from $i^{(\alpha\beta)}$ to $i_1^{(\alpha\beta)}$

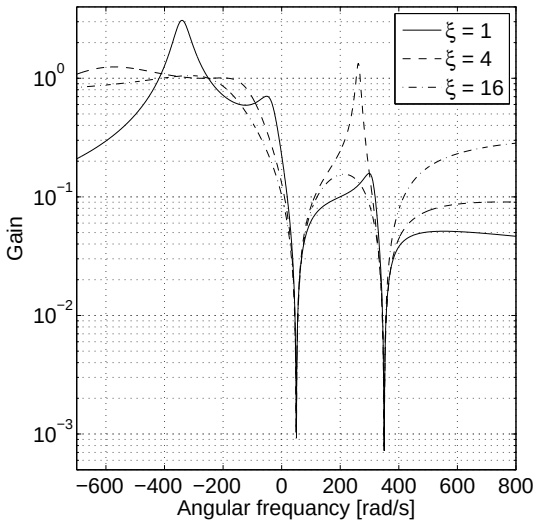

(c) Amplitude of frequency response from $i^{(\alpha\beta)}$ to $i_5^{(\alpha\beta)}$

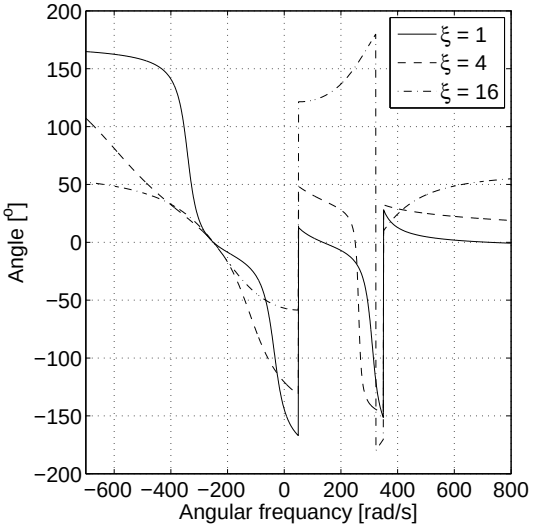

(d) Phase of frequency response from $i^{(\alpha\beta)}$ to $i_5^{(\alpha\beta)}$

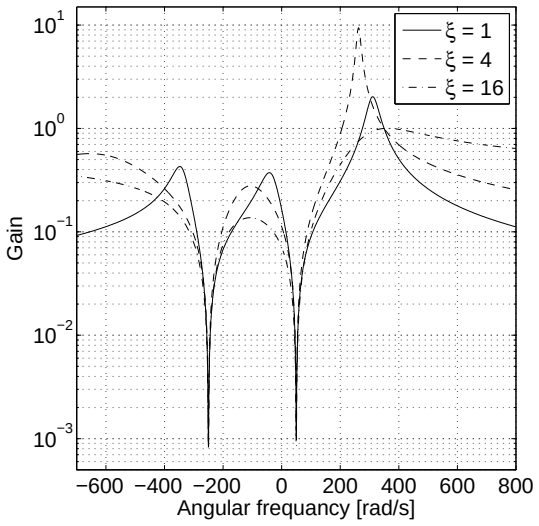

(e) Amplitude of frequency response from $i^{(\alpha\beta)}$ to $i_1^{(\alpha\beta)}$

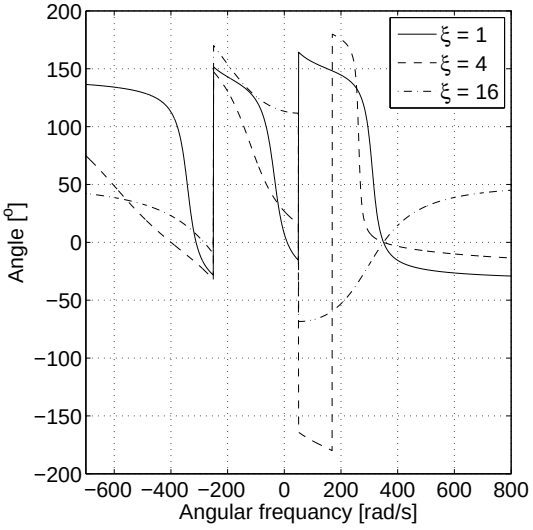

(f) Phase of frequency response from $i^{(\alpha\beta)}$ to $i_7^{(\alpha\beta)}$

Fig. 5.13 Frequency responce for $\omega_e = 50\ rad/s$

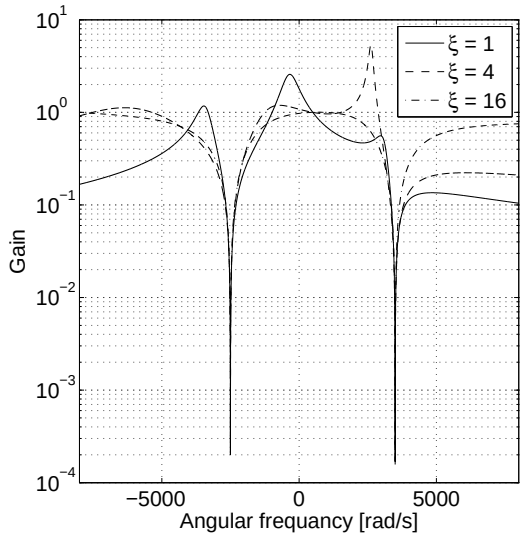

(a) Amplitude of frequency response from $i^{(\alpha\beta)}$ to $i_1^{(\alpha\beta)}$

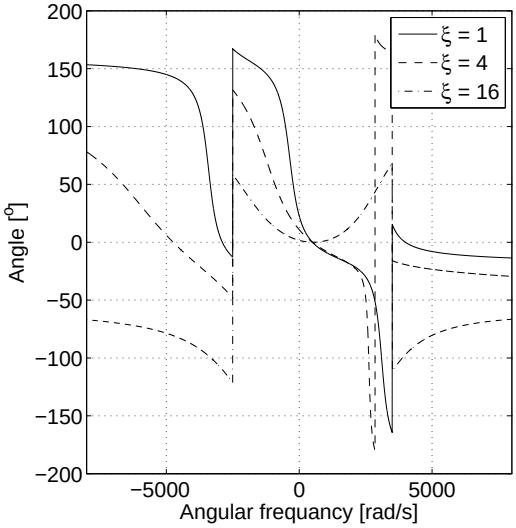

(b) Phase of frequency response from $i^{(\alpha\beta)}$ to $i_1^{(\alpha\beta)}$

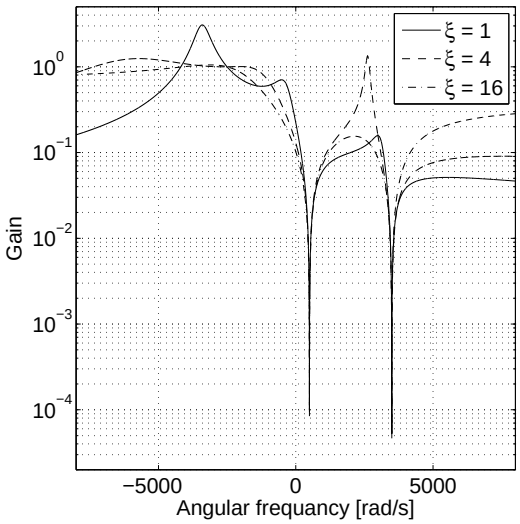

(c) Amplitude of frequency response from $i^{(\alpha\beta)}$ to $i_5^{(\alpha\beta)}$

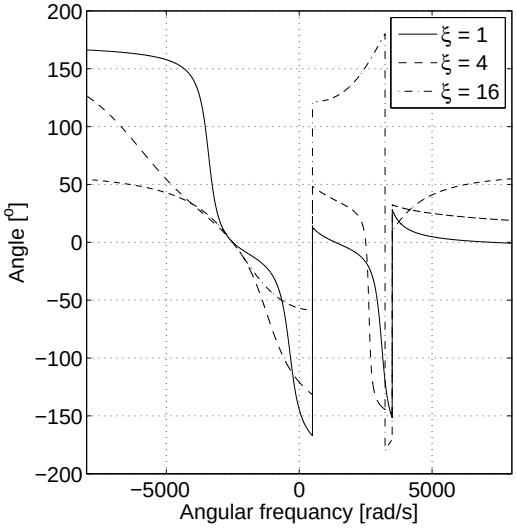

(d) Phase of frequency response from $i^{(\alpha\beta)}$ to $i_5^{(\alpha\beta)}$

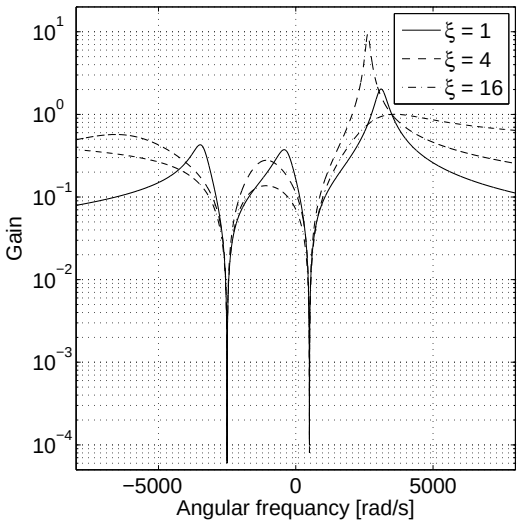

(e) Amplitude of frequency response from $i^{(\alpha\beta)}$ to $i_1^{(\alpha\beta)}$

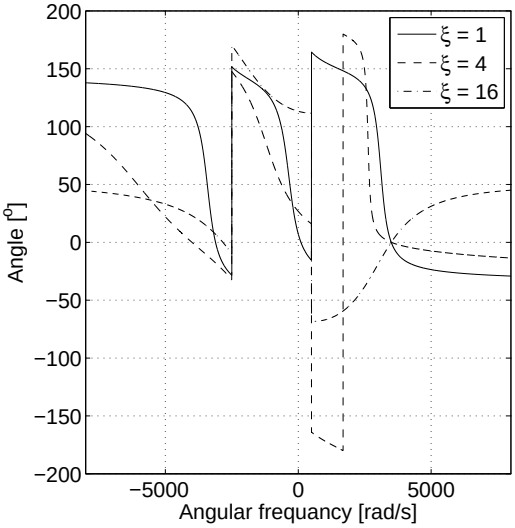

(f) Phase of frequency response from $i^{(\alpha\beta)}$ to $i_7^{(\alpha\beta)}$

Fig. 5.14 Frequency responce for $\omega_e = 500\ rad/s$

5.3 Traditional BLDC control

As already mentioned, the BLDC motor is traditionally controlled in a six step fashion. That is for each 60^o interval, two phases are actively carrying a current while the third phase does not. The activation of a phase is synchronized with the shape of its back emf, as seen in Figure 2.2(a)-2.2(b), and hence solely determined by rotor position.

By activating the phases according to this, the magnitude of the current can be controlled in a similar fashion as for a DC motor. The design approach that is going to be used is, also in this case, IMC. Therefore, according to the same motivation as for the PMSM, active damping and feed forward of back emf are utilized to improve the response from load disturbances. Observe however that the voltage that is going to be applied is the phase-to-phase voltage, and the back emf that is used for feed forward is therefore the phase-to-phase back emf. To sum up, the following model is obtained

$$2L\frac{di}{dt} = v' - 2(R + R_a)i \tag{5.37}$$

by choosing

$$v = v' - 2R_a i + 2\hat{k}\omega_e \tag{5.38}$$

5.3.1 Design of IMC controller

The design procedure of the IMC controller is identical as described for the PMSM and results in the following controller

$$F(p) = 2\alpha_c\hat{L} + \frac{2\alpha_c^2\hat{L}}{p} = k_p + \frac{k_i}{p} \tag{5.39}$$

5.3.2 Evaluation of current controller

To evaluate the performance of the current controller, a simulation of a step response is performed. The simulation is performed with the model of the ideal BLDC motor, adopting the parameters from the airplane motor. To achieve current waveforms close to the ideal ones, a very high bandwidth ($\alpha_c = 1\,000\,000\ rad/s$) of the current controller is utilized. The result is visualized in Figure 5.15(a)-5.15(c).

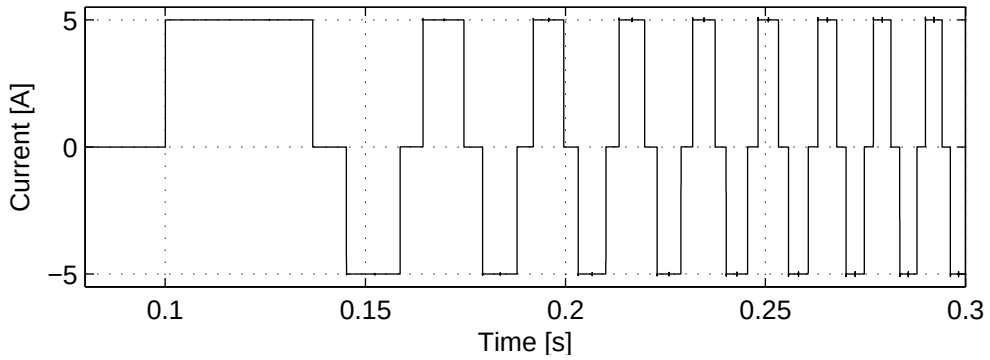

(a) i_a

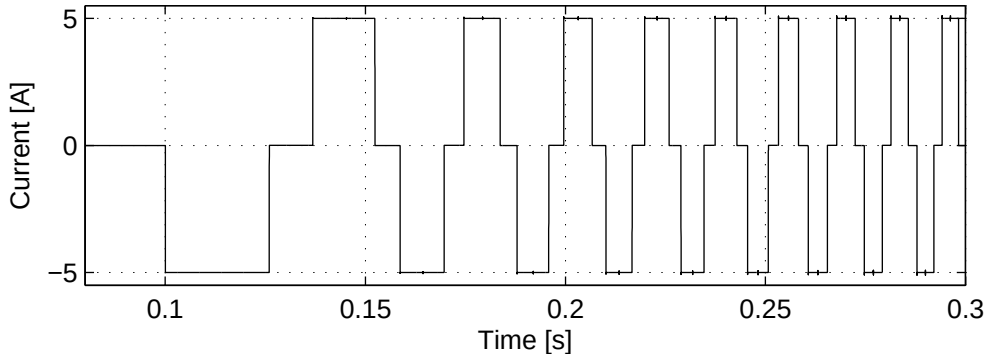

(b) i_b

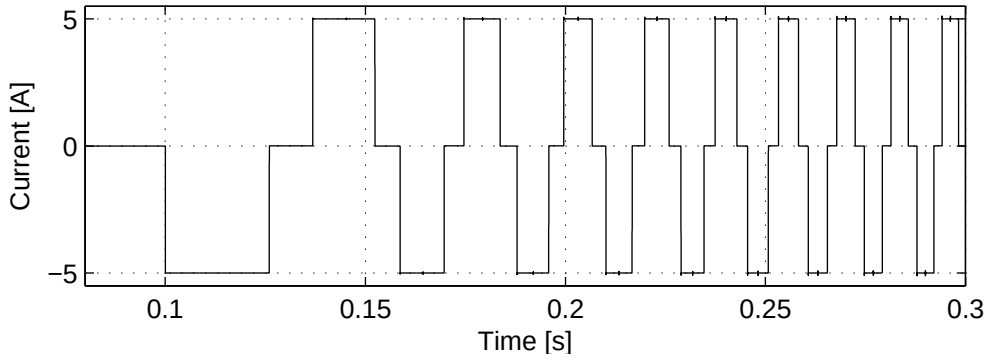

(c) i_c

Fig. 5.15 Step response. A step in the current reference to 5 A is performed at 0.1 s.

5.4 Advanced angle BLDC control

When the induced phase-to-phase back emf is close to the DC-link voltage, problems occur to achieve high current derivatives and hence the ideal current waveforms. This is one of the most severe disadvantages with the BLDC motor and will be discussed more in depth in Section 6.3 and in Section 7.2. There are however methods to reduce this problem [2], [11], [12], [13], [14], [15]. One way is to implement what often is referred to as *Lead Angle Adjustment* [13]. That is to compensate for the lag introduced by the inductance by modifying at which rotor position the commutation starts. In this application the motor is going to be used in a wide speed range and therefore it would be desirable to have an analytical expression for the angle θ_{lead} of which the commutation instance has to be changed.

The back emfs can be split as

$$e_x = e_{xz} + e_{zn} \tag{5.40}$$

where e_{zn} is the zero sequence and e_{xz} is the back emf in phase x with the zero sequence subtracted. By using this, (3.9) and (3.10) can be simplified to

$$\frac{di_a}{dt} = -\frac{R}{L}i_a + \frac{2}{3L}v_{ab} + \frac{1}{3L}v_{bc} - \frac{1}{L}e_{az} \tag{5.41}$$

$$\frac{di_b}{dt} = -\frac{R}{L}i_b - \frac{1}{3L}v_{ab} + \frac{1}{3L}v_{bc} - \frac{1}{L}e_{bz} \tag{5.42}$$

To obtain an analytical expression for θ_{lead}, commutation from phase A to phase B is studied. The following assumptions are also made

- The current increases and decreases linearly. This might seem to be a rough assumption, but it should be quite accurate for motors with a low resistance.
- $\frac{di_a}{dt} = -\frac{di_b}{dt}$. This is however only true at certain operating points, as will be explained in Section 7.2.
- It is also assumed that the current in phase B is the same after commutation as it was in phase A when the commutation started, hence $i_a(t_1) = i_b(t_2) = I$.

It is then straight forward to obtain the following by integrating (5.41) and (5.42)

$$I = \frac{3RI + 2v}{6L}(t_2 - t_1) + \frac{1}{L}\int_{t_1}^{t_2} e_{az}dt \tag{5.43}$$

$$I = \frac{-3RI + 4v}{6L}(t_2 - t_1) - \frac{1}{L}\int_{t_1}^{t_2} e_{bz}dt \tag{5.44}$$

where t_1 and t_2 are the time instants when the commutation begin and ends respectively. By realizing that $\int_{t_1}^{t_2} e_{az}dt = \int_{t_1}^{t_2} e_{bz}dt$ if the currents and back emfs are in phase, it is trivial to find the commutation time as

$$t_2 - t_1 = \frac{2LI}{v} \tag{5.45}$$

and hence θ_{lead} as

$$\theta_{lead} = \frac{t_2 - t_1}{2}\omega_e = \frac{\omega_e L I}{v} \tag{5.46}$$

5.4.1 Issues regarding implementation of lead angle adjustment

Equation (5.46) is not suitable for implementation since division by zero is possible. Therefore, since the problem is related to saturation in the output voltage, (5.46) is modified to

$$\theta_{lead} = \frac{\gamma_{lead}\omega_e L i_{ref}}{V_d} \tag{5.47}$$

where γ_{lead} is introduced as a design variable to enable tuning of θ_{lead}. It is also possible to observe that i_{ref} is used instead of I in (5.47), this is done to reduce the noise level in θ_{lead}.

Chapter 6

Comparison of torque ability

To quantify the difference between the motor types and the different control techniques regarding torque ability, the motor constant will be used. The motor constant is defined as [16]

$$k_m = \frac{T_e}{\sqrt{P_{loss}}} \tag{6.1}$$

where P_{loss} represent the resistive losses in the stator windings. As can be seen in (6.1) the motor constant is an indicator of at which cost torque can be produced, and hence an indicator of motor performance.

6.1 Theoretical differences between ideal permanent magnet motors

This section will present analytical expressions for motor constants for ideal BLDC motors and PMSMs.

6.1.1 Ideal BLDC motor

The obtained torque from an ideal BLDC motor is stated in (3.14) and can, in the ideal case, be simplified to

$$T_e = 2n_p\hat{k}\hat{i} \tag{6.2}$$

where $\hat{k}$ represents the peak value of the back emf shape and $\hat{i}$ represents the peak value of the stator current. The rms value of the ideal currents, visualized in Figure 2.2(b), is

$$I_{RMS} = \sqrt{\frac{2}{3}}\hat{i} \tag{6.3}$$

By using (6.2) and (6.3) an expression of the motor constant can be found to be

$$k_m = \sqrt{\frac{2}{R}}n_p\hat{k} \tag{6.4}$$

6.1.2 Ideal PMSM

In an ideal PMSM both the currents and the back emf shapes are sinusoidal and in phase. By using this in (3.14) the produced torque can be expressed as

$$T_e = \frac{3}{2} n_p \hat{k} \hat{i} \tag{6.5}$$

The motor constant can then easily be found to be

$$k_m = \sqrt{\frac{3}{2R}} n_p \hat{k} \tag{6.6}$$

By comparing (6.4) and (6.6) it can be realized that an ideal BLDC motor has almost 15.5% higher motor constant than an ideal PMSM. The difference will however be smaller in reality due to difficulties to create the ideal back emfs and the ideal currents for the BLDC motor.

Theoretical calculated motor constants for ideal motors with parameters adopted from the Airplane motor and BLDC motor are stated in Table 6.1 and Table 6.2 respectively.

Table 6.1: Theoretical motor constants for ideal motors with parameters from the Airplane motor

Motor type	k_m $[Nm/W^{1/2}]$
PMSM	1.0245
BLDC	1.1830

Table 6.2: Theoretical motor constants for ideal motors with parameters from the BLDC motor

Motor type	k_m $[Nm/W^{1/2}]$
PMSM	1.5313
BLDC	1.7681

6.2 Simulation results

The aim of this section is to compare the performance of the motors when sinusoidal and traditional BLDC commutation are utilized. It is therefore desirable to achieve current waveforms as close as possible to the ideal current shapes. For the BLDC motor it will also be investigated how the motor perform if the current has the same shape as the back emf.

6.2.1 Airplane motor

Traditional BLDC control

To achieve current waveforms close to the ideal ones, the bandwidth of the current controller is chosen to be very high ($\alpha_c = 1\,000\,000 rad/s$). The obtained torque and currents,

from a unity step response, are visualized in Figure 6.2 and Figure 6.1(a)-6.1(c) respectively. The obtained motor constant is presented in Table 6.3.

Table 6.3: Simulation results

$T_{e,avg}\ [Nm]$	0.1087
$P_{loss}\ [W]$	0.0130
$k_m\ [Nm/W^{1/2}]$	0.9543

First, it is possible to observe that the current waveforms are close to the ideal shapes but the obtained torque is not. This is since the back emfs are far from the ideal shapes for a BLDC motor. The motor constant is, as a result, substantially (almost 20%) lower than for an ideal BLDC motor.

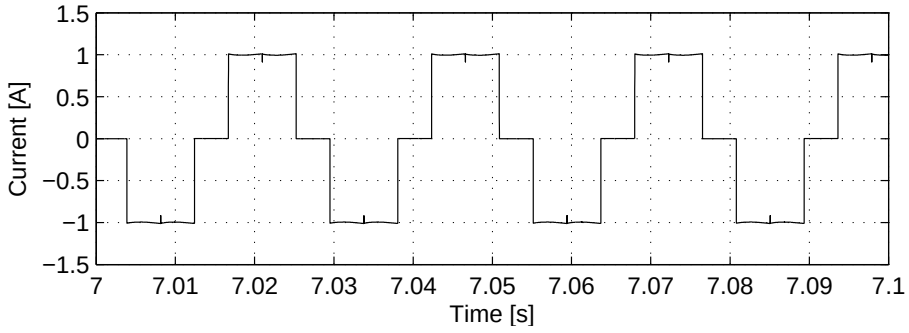

(a) i_a

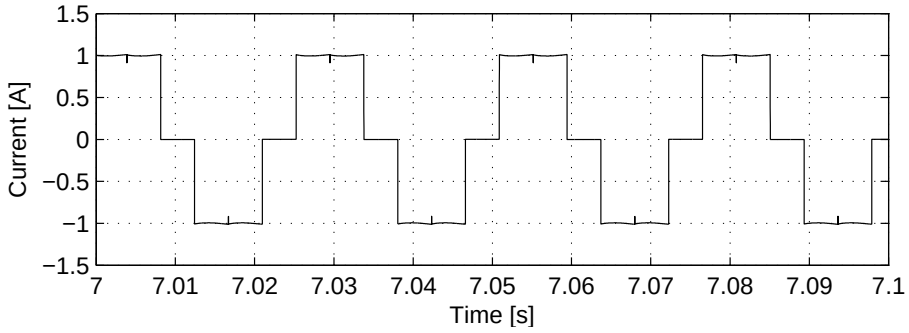

(b) i_b

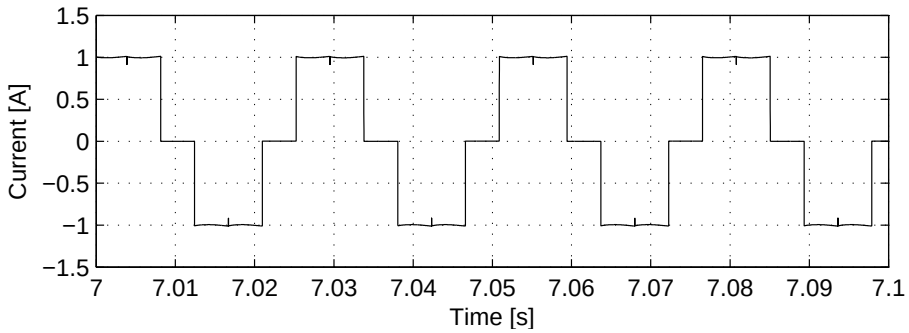

(c) i_c

Fig. 6.1 Currents in steady state

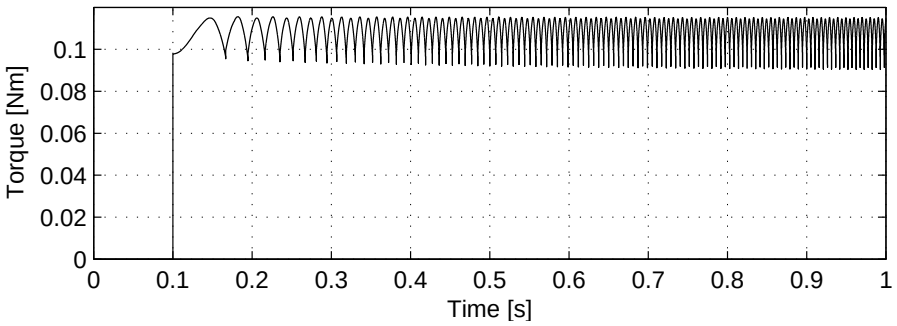

Fig. 6.2 Produced torque

Field oriented control

To obtain sinusoidally shaped currents, feed forward of the true back emf is utilized. The torque and currents, from a unity step response in the q-current, are visualized in Figure 6.3 and Figure 6.4(a)-6.4(c) respectively. The motor constant is presented in Table 6.4.

Table 6.4: Simulation results

$T_{e,avg}\ [Nm]$	0.0986
$P_{loss}\ [W]$	0.0097
$k_m\ [Nm/W^{1/2}]$	1.0005

Observe that the currents are very close to sinusoidal shapes and that the motor constant is close to the calculated for an ideal PMSM. A motor constant close to an ideal PMSM is quite natural since the back emfs are more or less sinusoidally shaped. It is also possible to note that the motor constant is higher when the motor is controlled as a PMSM compared to when it is controlled as a BLDC motor. The obtained average torque for the same peak value of the current is, however, higher for the BLDC control.

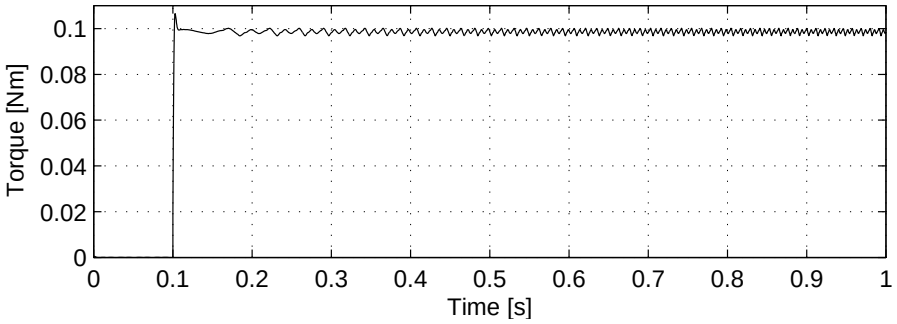

Fig. 6.3 Produced torque

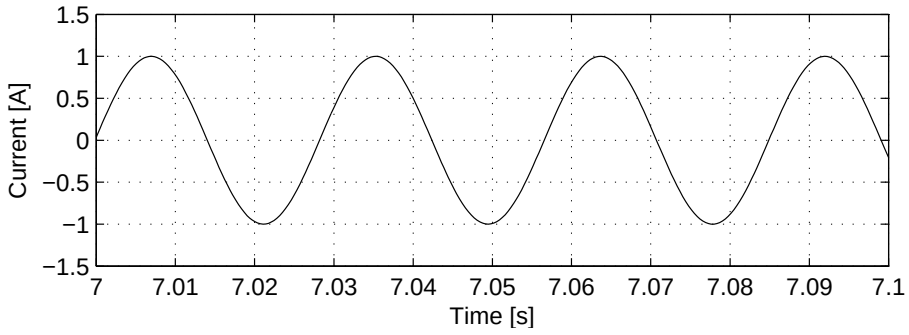

(a) i_a

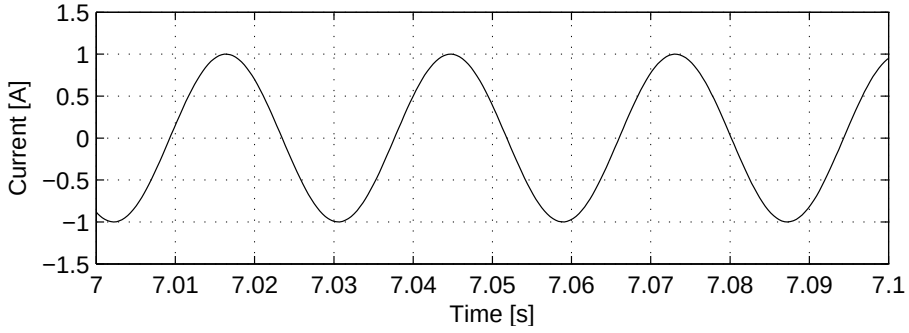

(b) i_b

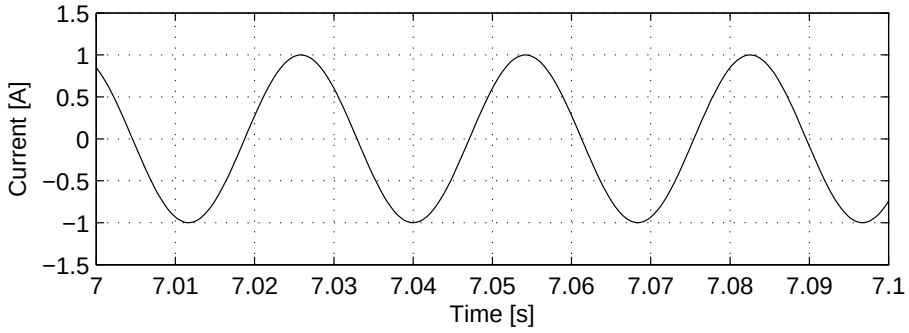

(c) i_c

Fig. 6.4 Currents in steady state

6.2.2 BLDC motor

Traditional BLDC control

To achieve current waveforms close to the ideal ones, the bandwidth of the current controller is also in this case chosen to be very high ($\alpha_c = 1\,000\,000\ rad/s$). The obtained torque and currents, from a unity step response, are visualized in Figure 6.5 and Figure 6.6(a)-6.6(c) respectively. The obtained motor constant is presented in Table 6.5.

Table 6.5: Simulation results

$T_{e,avg}\ [Nm]$	1.7113
$P_{loss}\ [W]$	1.2977
$k_m\ [Nm/W^{1/2}]$	1.5022

The motor constant is, also in this case, lower (about 15%) than the ideal motor con-

stant for a BLDC motor. It is however, as expected, closer to the ideal case than it was for the Airplane motor.

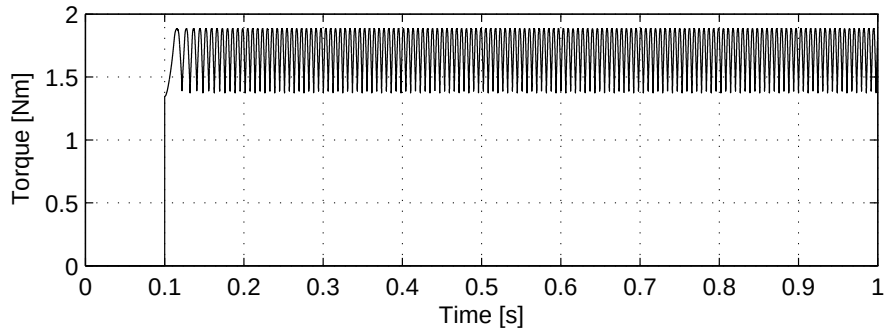

Fig. 6.5 Produced torque

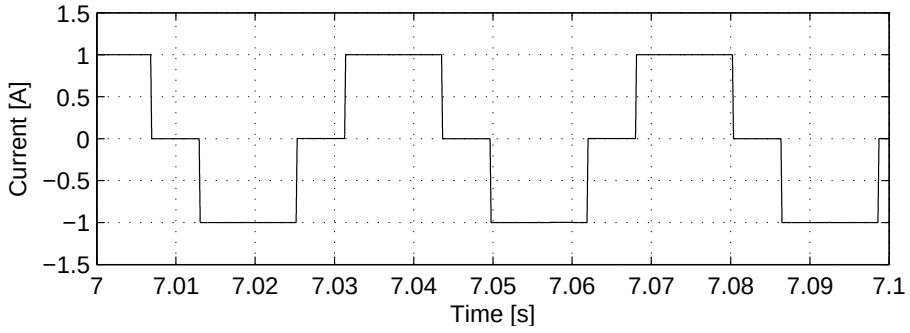

(a) i_a

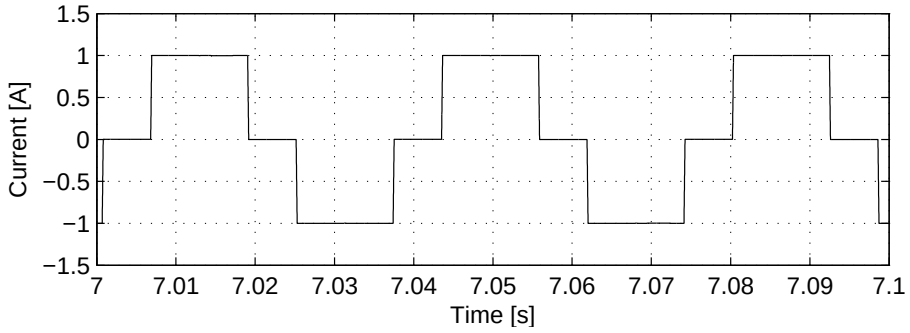

(b) i_b

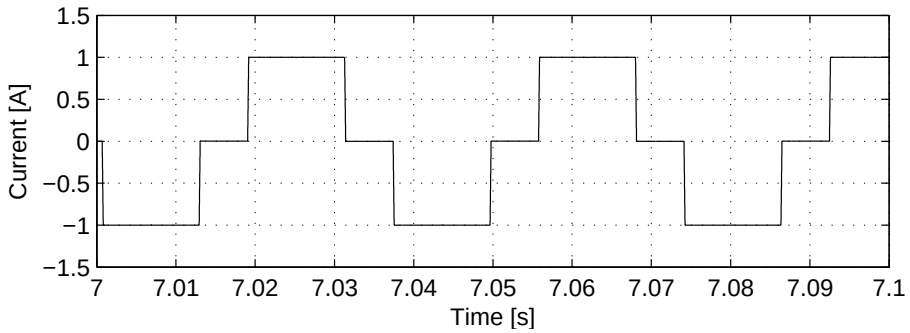

(c) i_c

Fig. 6.6 Currents in steady state

Field oriented control

To obtain sinusoidally shaped currents, feed forward of the true back emf is utilized. The torque and currents, from a unity step response in the q-current, are visualized in Figure 6.8 and Figure 6.7(a)-6.7(c) respectively. The motor constant is presented in Table 6.6.

The obtained motor constant is close to the motor constant for an ideal PMSM. It is also possible to observe that the motor constant, also for this motor, is higher when controlled as a PMSM compared to BLDC control. The difference is however smaller compared to the Airplane motor. Moreover, the obtained average torque per peak current is 11.5% higher when BLDC control is utilized compared to FOC.

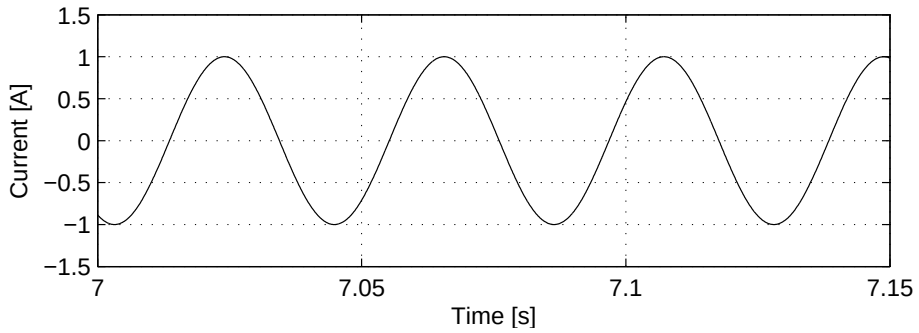

(a) i_a

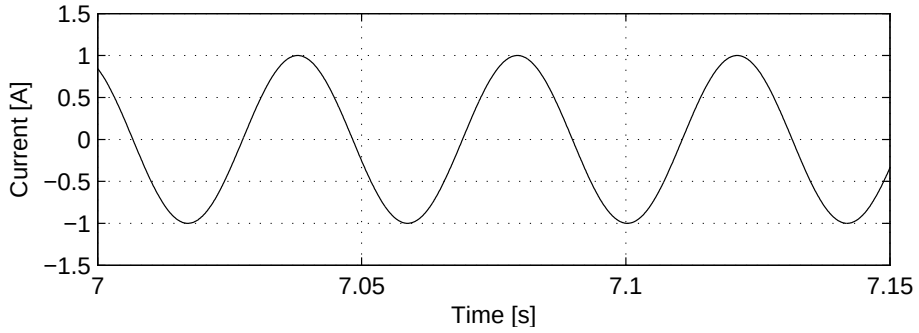

(b) i_b

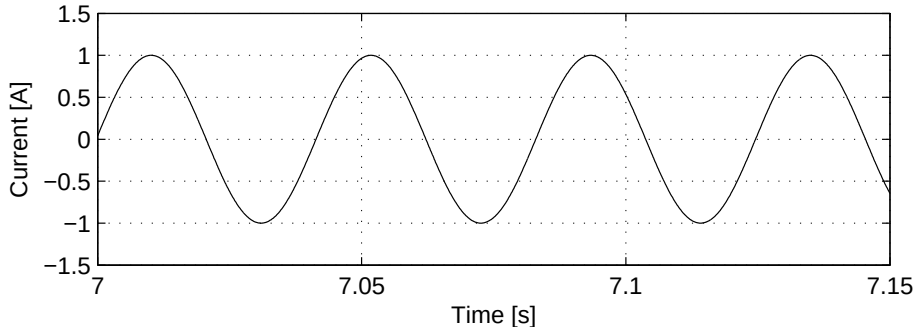

(c) i_c

Fig. 6.7 Currents in steady state

Table 6.6: Simulation results

$T_{e,avg}\ [Nm]$	1.5130
$P_{loss}\ [W]$	0.9741
$k_m\ [Nm/W^{1/2}]$	1.5330

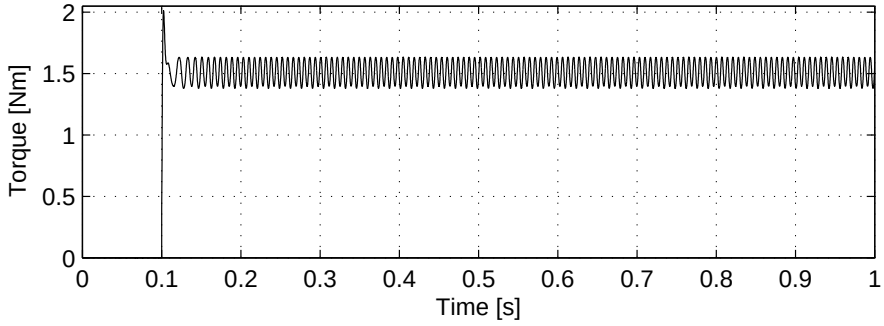

Fig. 6.8 Produced torque

Field oriented control of harmonics

To evaluate the performance of the control scheme, a unit reference step in the fundamental current is performed. The references of the harmonics are calculated according to (5.9) and (5.10). The obtained torque and currents are visualized in Figure 6.9 and Figure 6.10(a)-6.10(c) respectively. The obtained motor constant is presented in Table 6.7.

Table 6.7: Simulation results

$T_{e,avg}\ [Nm]$	1.5326
$P_{loss}\ [W]$	0.9912
$k_m\ [Nm/W^{1/2}]$	1.5394

It is evident from Table 6.7 that it is possible to achieve a higher motor constant with this method than with traditional BLDC or PMSM control. The obtained motor constant is higher than for an ideal PMSM but lower than for an ideal BLDC motor. This is natural since more harmonics is utilized to produce torque than for an ideal PMSM but less than for an ideal BLDC motor.

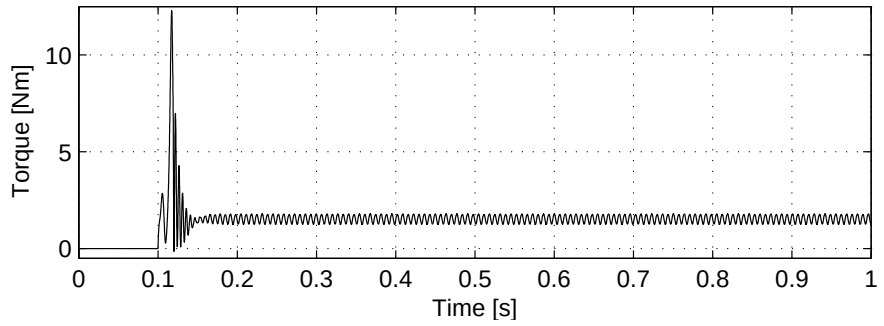

Fig. 6.9 Produced torque

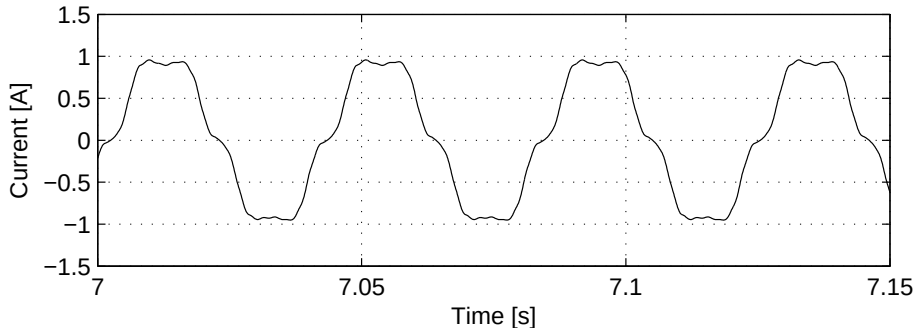

(a) i_a

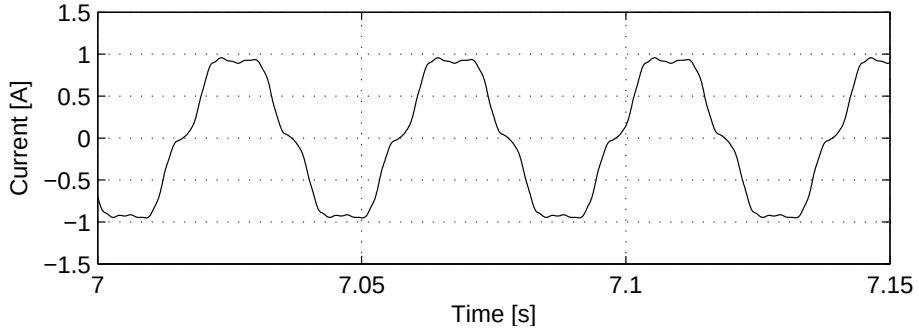

(b) i_b

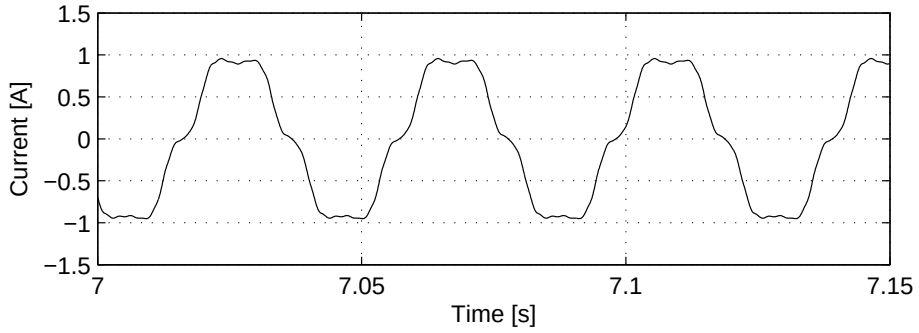

(c) i_c

Fig. 6.10 Currents in steady state

6.3 Effects of torque ripple due to phase commutation in BLDC motors

Up to this point, it has been assumed that the controller has access to unlimited amounts of voltage. In reality it is however not possible to have an output voltage higher than the DC-link voltage. This causes problems to obtain high current derivatives and hence problems to achieve the desired current waveforms. Especially when the induced phase-to-phase back emf is close to the DC-link voltage. As a result there will often be ripple in the torque due to phase commutation. This section will present an example of how this affects the motor constant as well as a method to reduce the problem. A theoretical analysis of torque ripple due to this problem will be presented in Section 7.2, where the ripple in the example presented below also is quantified.

6.3.1 An example

To illustrate this problem, a simulation where the voltage is limited to $70\,V$ is performed. The model utilized is of the ideal BLDC motor with parameters from the Airplane motor. The induced back emfs are visualized in Figure 6.12(a)-6.12(c), where it is possible to observe that the magnitudes are slightly less than $35\,V$ ($32.87\,V$). The induced phase-to-phase voltages are hence close to the DC-link voltage. The phase currents are visualized in Figure 6.13(a)-6.13(c) and the obtained torque are visualized in Figure 6.11. The motor constant is presented in Table 6.8.

Table 6.8: Simulation results

$T_{e,avg}\ [Nm]$	2.0879
$P_{loss}\ [W]$	3.2072
$k_m\ [Nm/W^{1/2}]$	1.1658

The current waveforms in Figure 6.13(a)-6.13(c) obviously deviate from the ideal shapes. As a result there is ripple in the torque. Also, the obtained motor constant is lower than for an ideal BLDC motor since a higher RMS-current is needed to have the same average torque. The torque ripple visualized in Figure 6.11 will be quantified in Section 7.2.

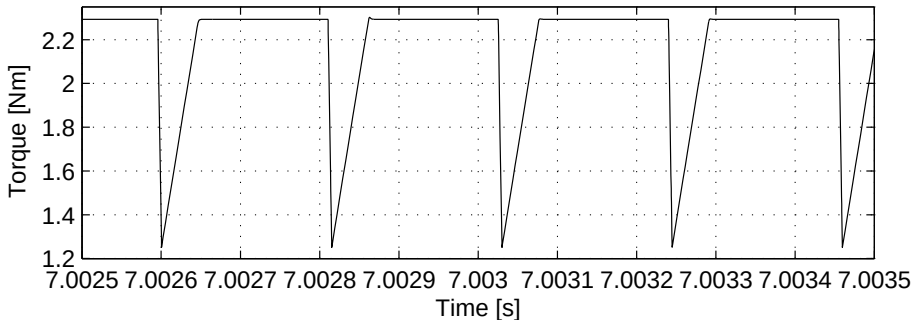

Fig. 6.11 Produced torque

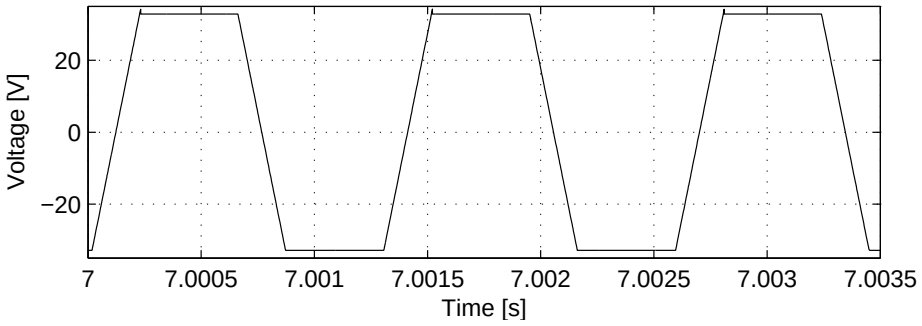

(a) e_a

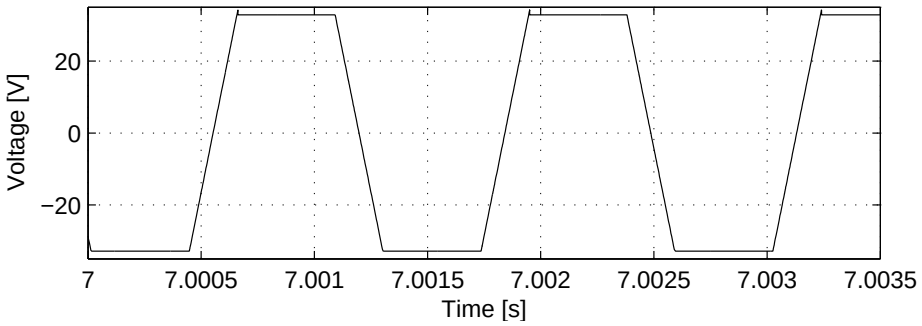

(b) e_b

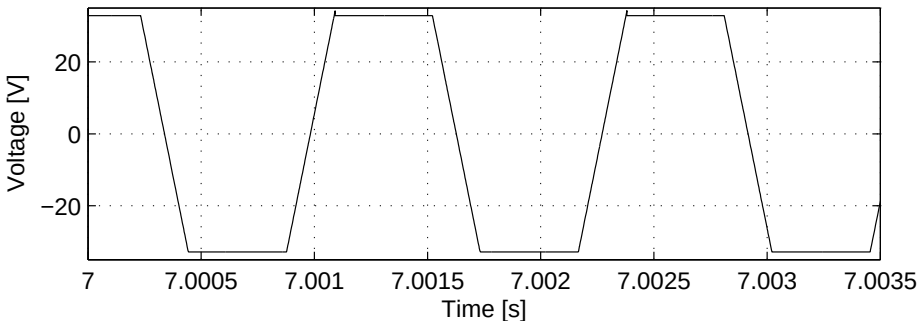

(c) e_c

Fig. 6.12 Back emfs in steady state

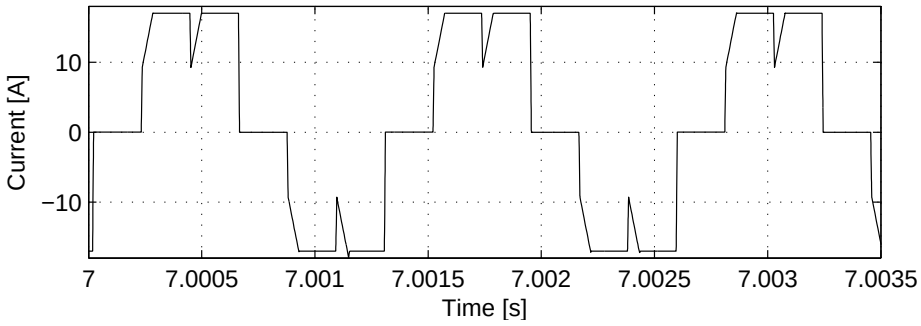

(a) i_a

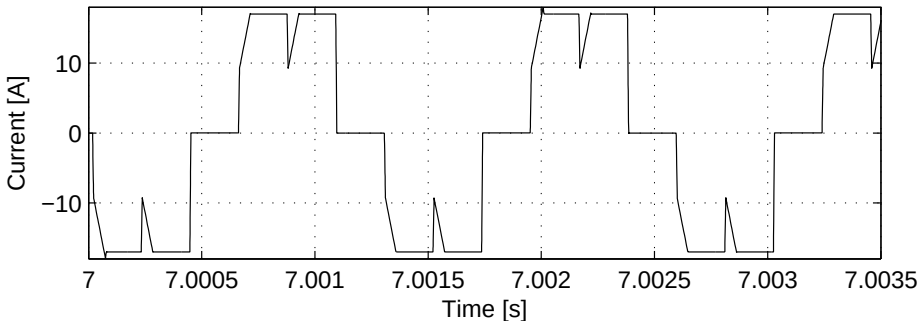

(b) i_b

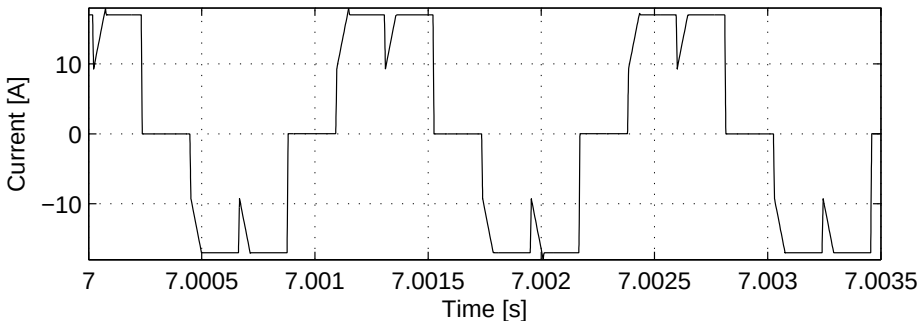

(c) i_c

Fig. 6.13 Currents in steady state

6.3.2 Advanced angle BLDC control

To illustrate how the problem with phase commutation at high speeds can be reduced, the same simulation as in Section 6.3.1 is performed with lead angle adjustment. By comparing the results in Table 6.9 and Table 6.8, it can be noted that the motor constant can be increased by utilizing lead angle adjustment.

Table 6.9: Simulation results

γ_{lead}	1	2
$T_{e,avg}\ [Nm]$	2.1012	2.1009
$P_{loss}\ [W]$	3.2277	3.2301
$k_m\ [Nm/W^{1/2}]$	1.1695	1.1689

The phase currents and the torque, in steady state, for $\gamma_{lead} = 1$ are visualized in Figure 6.16(a)-6.16(c) and Figure 6.14 respectively. The back emfs and the lead angle are visualized in Figure 6.17(a)-6.17(c) and Figure 6.15. Also in this case, the torque ripple visualized in Figure 6.14 will be quantified in Section 7.2.

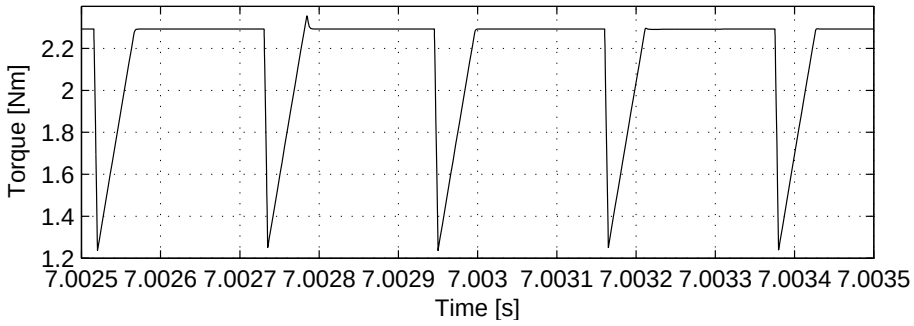

Fig. 6.14 Produced torque

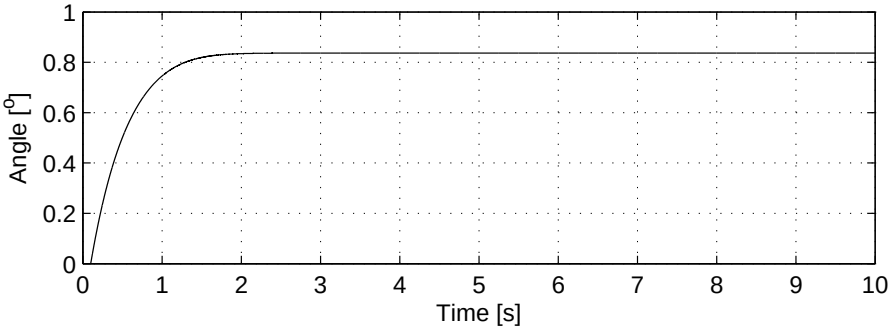

Fig. 6.15 θ_{lead}

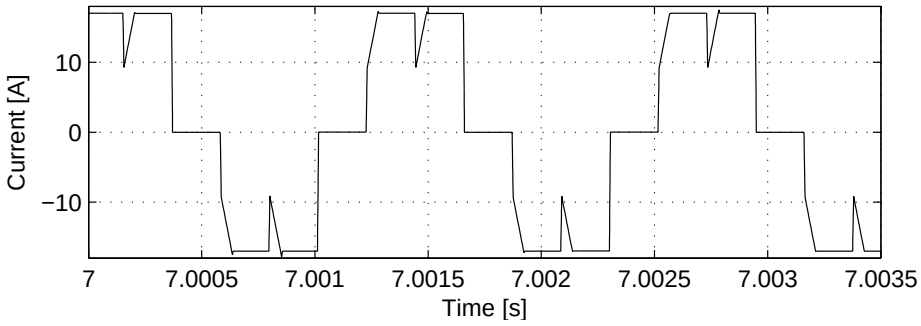

(a) i_a

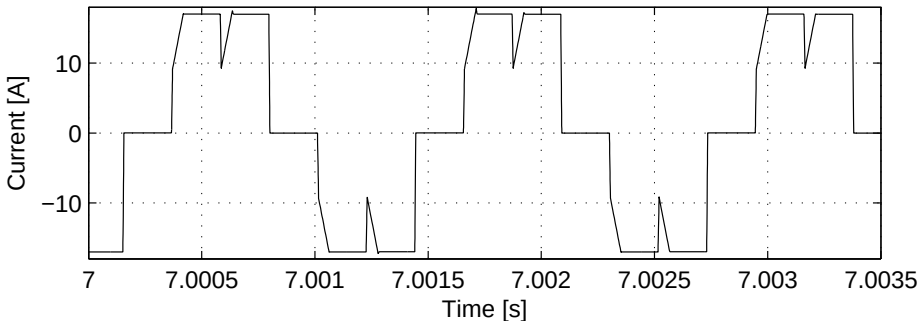

(b) i_b

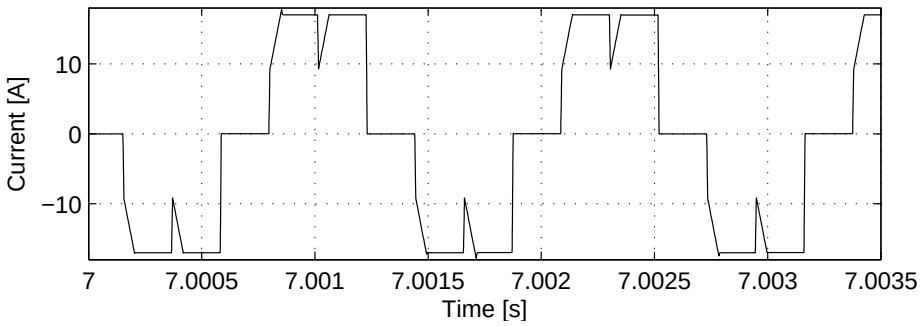

(c) i_c

Fig. 6.16 Currents in steady state

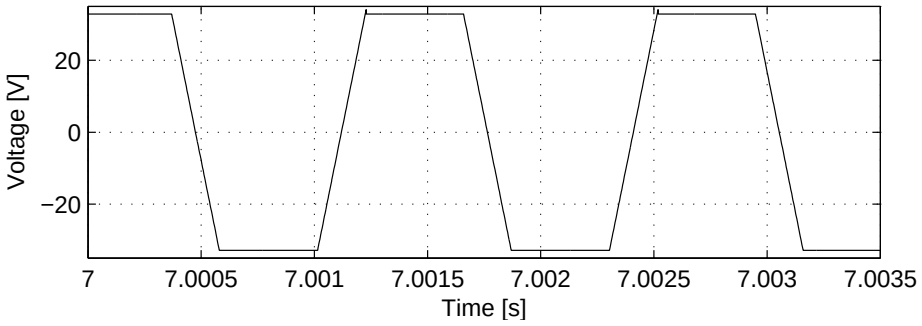

(a) e_a

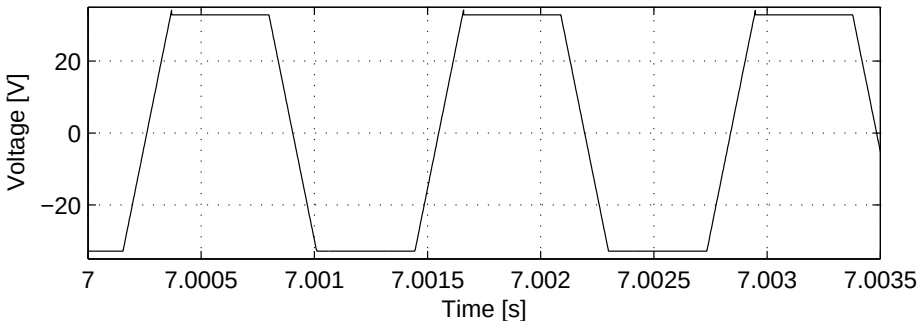

(b) e_b

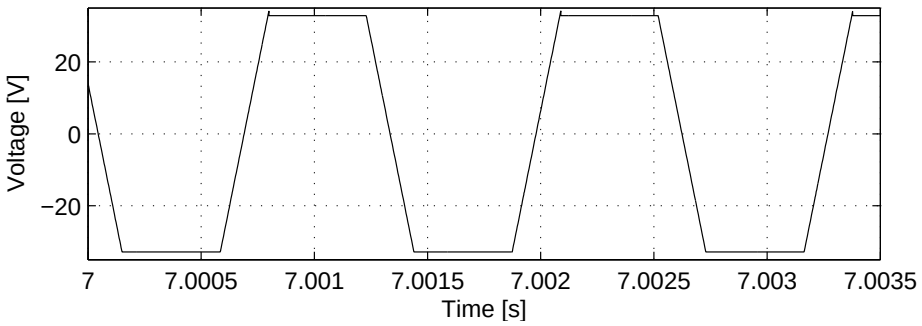

(c) e_c

Fig. 6.17 Back emfs in steady state

Chapter 7

Comparison of torque ripple

The torque produced by a permanent magnet motor can be divided into three different components

- Torque due to interaction between rotor and stator magnetic fields.
- Reluctance torque due to saliency.
- Cogging torque.

In this chapter ripple due to interaction between rotor and stator magnetic fields will be investigated.

To quantify the difference between the motor types and control techniques regarding torque ripple, the *relative torque ripple* in steady state will be studied. The relative torque ripple is defined as

$$\Delta T_e = \frac{T_{e,ripple,peak-to-peak}}{T_{e,avg}} \tag{7.1}$$

7.1 Simulation results

The aim of this section is to compare the ripple in the produced torque when the motors are controlled with the different control techniques.

7.1.1 Airplane motor

In this section, the torque ripple, obtained from the simulations in the corresponding subsections in 6.2.1, will be studied.

Traditional BLDC control

The torque ripple in steady state is visualized in Figure 7.1 and the relative torque ripple is presented in Table 7.1. Since the currents are close to the ideal shapes, there is torque ripple since the back emfs deviate from the ideal waveforms.

Table 7.1: Simulation results

$T_{e,avg}\ [Nm]$	0.1087
$T_{e,ripple,peak-to-peak}\ [Nm]$	0.0255
ΔT_e	0.2346

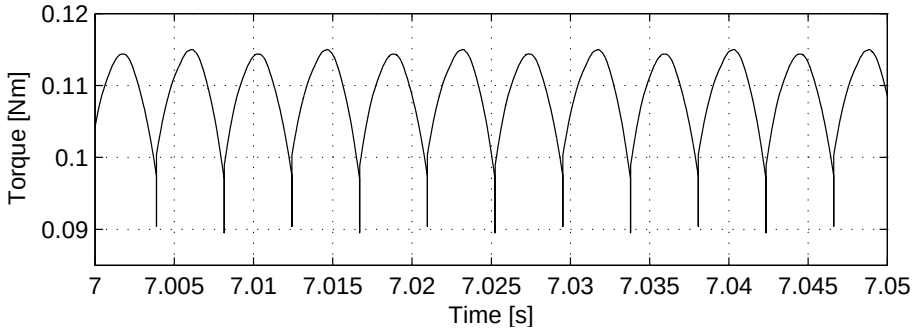

Fig. 7.1 Produced torque

Field oriented control

The torque ripple in steady state is visualized in Figure 7.2 and the relative torque ripple is presented in Table 7.2. Observe that the relative torque ripple is much lower when the motor is controlled as a PMSM compared to when it is controlled as a BLDC motor. This is quite natural since the back emfs are close to sinusoidal shapes.

Table 7.2: Simulation results

$T_{e,avg}\ [Nm]$	0.0986
$T_{e,ripple,peak-to-peak}\ [Nm]$	0.0033
ΔT_e	0.0332

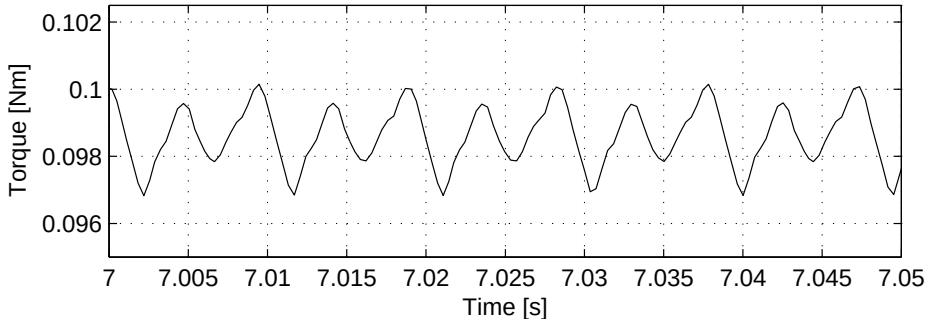

Fig. 7.2 Produced torque

7.1.2 BLDC motor

In this section, the torque ripple, obtained from the simulations in the corresponding subsections in 6.2.2, will be studied.

Traditional BLDC control

The torque ripple in steady state is visualized in Figure 7.3 and the relative torque ripple is presented in Table 7.3.

Table 7.3: Simulation results

$T_{e,avg}\ [Nm]$	1.7113
$T_{e,ripple,peak-to-peak}\ [Nm]$	0.5109
ΔT_e	0.2985

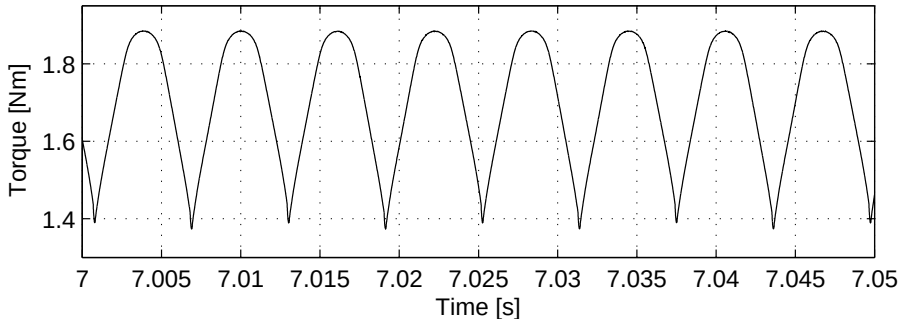

Fig. 7.3 Produced torque

Field oriented control

The torque ripple in steady state is visualized in Figure 7.4 and the relative torque ripple is presented in Table 7.4. Observe that the relative torque ripple is, also for this motor, lower when it is controlled as a PMSM. The difference is however smaller than it is for the Airplane motor.

Table 7.4: Simulation results

$T_{e,avg}\ [Nm]$	1.5130
$T_{e,ripple,peak-to-peak}\ [Nm]$	0.2531
ΔT_e	0.1673

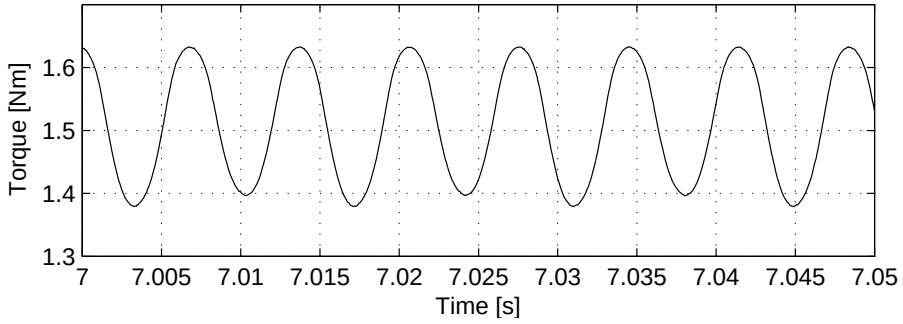

Fig. 7.4 Produced torque

Field oriented control of harmonics

The torque ripple is visualized in Figure 7.5 and the relative torque ripple is presented in Table 7.5. Observe that this method produces a higher relative (and absolute) torque ripple than the traditional BLDC and PMSM control.

Table 7.5: Simulation results

$T_{e,avg}\ [Nm]$	1.5326
$T_{e,ripple,peak-to-peak}\ [Nm]$	0.5433
ΔT_e	0.3545

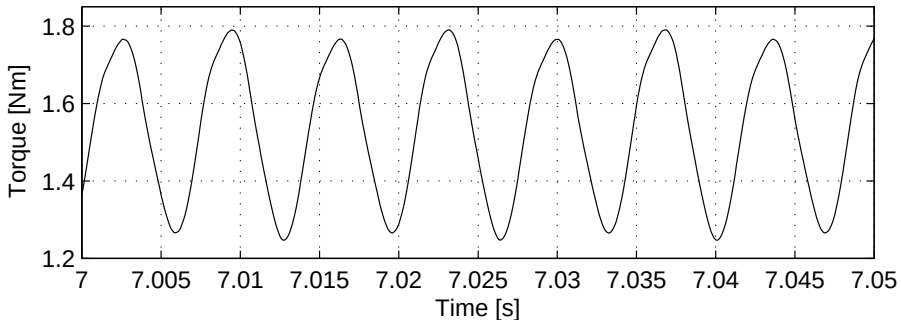

Fig. 7.5 Produced torque

7.2 Effects of torque ripple due to phase commutation in BLDC motors

This section will describe the torque ripple due to phase commutation in BLDC motors. A short analytical analysis will be presented. Furthermore, the relative torque ripple in the example presented in Section 6.3 will be quantified.

7.2.1 Analytical analysis of torque ripple due to phase commutation

A short analysis of the commutation torque ripple will here be performed since analytical expressions often are valuable to gain a conceptual understanding.

Consider commutation from phase A to phase B for an ideal BLDC motor. The back emfs during commutation are then

$$e_a = e_b = -e_c = \hat{e} \tag{7.2}$$

where $\hat{e}$ is the peak value of the back emfs. By using this in (3.14) it is evident that the torque during commutation is given by

$$T_e = -2n_p\hat{k}i_c \tag{7.3}$$

The torque during commutation is hence proportional to the noncommutating phase current i_c.

By observing from Table 3.1 that during commutation

$$v_{ab} = -v_{bc} = -v \tag{7.4}$$

(3.9) and (3.10) can be simplified to

$$\frac{di_a}{dt} = -\frac{R}{L}i_a - \frac{v - 2\hat{e}}{3L} \tag{7.5}$$

$$\frac{di_b}{dt} = -\frac{R}{L}i_b + \frac{2(v - \hat{e})}{3L} \tag{7.6}$$

By using (7.5), (7.6) and (3.11), it is evident that

$$\frac{di_c}{dt} = -\frac{R}{L}i_c - \frac{v - 4\hat{e}}{3L} \tag{7.7}$$

which indicates that commutation ripple depends on the relation between back emf and DC-link voltage. A more thoroughly analysis of commutation ripple is found in [17]. By neglecting the resistance, the commutation ripple can be divided into three different cases depending on the operating point [17]. Observe that this is also obvious in (7.7).

- $v = 4\hat{e}$. This will cause $\frac{di_c}{dt} = 0$, and hence eliminating the commutation ripple.
- $v < 4\hat{e}$ will result in a dip in the produced torque during commutation.
- $v > 4\hat{e}$ will result in a peak in the produced torque during commutation.

The torque dip in the second case is given by [17]

$$T_{e,dip} = \frac{2\hat{e}I}{\omega_m}(1 + \frac{v - 4\hat{e}}{v + 2\hat{e}}) \tag{7.8}$$

By using (7.8) and (6.2) the average torque can be found to be

$$T_{e,avg,2} = \frac{6\hat{e}I}{\pi\omega_m}(\frac{\pi}{3} + \omega_m t_{com,2}\frac{v - 4\hat{e}}{2(v + 2\hat{e})}) \tag{7.9}$$

where $t_{com,2}$ represents the commutation time and is given by [17]

$$t_{com,2} = \frac{LI}{v + 2\hat{e}} \tag{7.10}$$

It is also clear that

$$T_{e,ripple,peak-to-peak} = T_{e,dip} \tag{7.11}$$

Similarly, if the same analysis is performed for the third case, the following results are obtained. The average torque can be expressed as

$$T_{e,avg,3} = \frac{6\hat{e}}{\pi\omega_m}(\frac{\pi}{3} + \omega_m t_{com,3}\frac{v - 4\hat{e}}{4(v - \hat{e})}) \tag{7.12}$$

where $t_{com,3}$ represents the commutation time and is given by [17]

$$t_{com,3} = \frac{LI}{v - 2\hat{e}} \tag{7.13}$$

The torque peak is given by [17]

$$T_{e,ripple,peak,to-peak} = T_{e,peak} = \frac{2\hat{e}I}{\omega_e}(1 + \frac{v - 4\hat{e}}{2(v - \hat{e})}) \tag{7.14}$$

7.2.2 An example

This section will quantify the torque ripple due to phase commutation in the simulation described in Section 6.3.1. The torque ripple is visualized in steady state in Figure 6.11 and the relative torque ripple is presented in Table 7.6. The relative torque ripple due to phase commutation is in this example more severe than any of the previously presented cases for ideal current waveforms. Furthermore, recall from Section 6.3.1 that this phenomenon also decreases the motor constant. This illustrates that phase commutation in many cases is a severe problem with BLDC motors.

Table 7.6: Simulation results

$T_{e,avg}\ [Nm]$	2.0879
$T_{e,ripple,peak-to-peak}\ [Nm]$	1.0412
ΔT_e	0.4987

It is also interesting to see how well the ripple can be predicted by (7.8)-(7.11). By using that $v = 70\ V$ during commutation, the peak values of the back emfs are $32.87\ V$, the peak values of the currents are $17\ A$ and that the mechanical speed is $487.7\ rad/s$, it is possible to find the values presented in Table 7.7. The predictions correspond quite well with the simulation even though the resistance is neglected in the derivation of (7.8)-(7.11).

Table 7.7: Prediction

$T_{e,avg}\ [Nm]$	2.2912
$T_{e,ripple,peak-to-peak}\ [Nm]$	1.2537
ΔT_e	0.5472

7.2.3 Advanced angle BLDC control

This section will quantify the ripple in the simulations described in Section 6.3.2. The torque in steady state is visualized for $\gamma_{lead} = 1$ in Figure 6.14. It can be noted from Table 7.8 that this method has a low impact on the relative torque ripple in these simulations. It should however be noted from Figure 6.15 that the lead angle is quite small. A theoretical analysis of the harmonic content in the torque due to phase advancing is performed in [18], from which it is clear that lead angle adjustment, not only decreases the available torque, but also increases torque harmonic content substantially.

Table 7.8: Simulation results

γ_{lead}	1	2
$T_{e,avg}\ [Nm]$	2.1012	2.1009
$T_{e,ripple,peak-to-peak}\ [Nm]$	1.0556	1.0393
ΔT_e	0.5024	0.4947

Chapter 8

Concluding remarks and future work

8.1 Summary and concluding remarks

The aim of the work was to investigate how two existing permanent magnet motors perform when different control techniques are used. To do so, ideal models of a BLDC motor and a PMSM have been adapted to two permanent magnet motors. The motor constant as well as the relative torque ripple has been studied when different control techniques are utilized.

Even though an ideal BLDC motor has a higher motor constant than an ideal PMSM, simulations showed that a higher motor constant (almost 5% and about 2% for the two motors respectively) can be obtained by utilizing FOC compared to traditional BLDC control. A lower relative torque ripple (almost 86% and almost 44% for the two motors respectively) was also obtained for FOC compared to traditional BLDC control. It should however be noted that a higher average torque per peak current was obtained with traditional BLDC control.

A higher motor constant indicates that the efficiency might be higher. It should however be noted that the motor constant only takes resistive losses in the stator windings into account. For instance, it has been shown that a motor can have an overall efficiency that is higher when it is controlled as a BLDC motor compared to FOC, especially at light loads [2]. Mainly since the iron losses (which are neglected in this work) can be lower when traditional BLDC control is utilized [2].

A novel control scheme to control the currents to have the same shape as the back emfs was presented. The control scheme is utilizing an RLS-algorithm to find the fundamental component and the most significant harmonics in the measured current. Field oriented control is then utilized for the fundamental and the harmonics. This technique was only implemented for the motor with the highest amount of harmonics in the back emf.

Simulations showed that it is possible to obtain a higher motor constant, compared to both FOC and traditional BLDC control, by controlling the currents to have the same shape as the back emfs. For the investigated case, simulations showed, however, a less than 1% increase in motor constant with this method compared to FOC. The relative torque ripple was increased by using this method. In fact, the highest relative (and absolute) torque ripple was obtained with this method. Simulations also showed that the average torque per peak current was higher for this method compared to standard FOC, but lower than for traditional BLDC control.

The effects of torque ripple due to phase commutation for traditional BLDC control was illustrated with an example as well as an analytical analysis. Simulations showed that the ripple due to phase commutation can be severe even for an ideal BLDC motor. The torque ripple was in fact more severe than for any of the simulations, with ideal current waveforms, of a corresponding non ideal motor. As a result the motor constant decreased and the relative torque ripple increased.

A well known method to reduce the problem with phase commutation is lead angle adjustment. A version of this approach was derived and implemented. The method was successful in increasing the motor constant for the example used to illustrate the problem. The relative torque ripple was more or less unaffected, but it should be stated that the lead angle for the specific example was small.

8.2 Future work

This section will present ideas for future work related to this thesis.

- Firstly, it would of course be interesting to verify the results by laboratory tests.
- The FOC of harmonics should, with only minor modifications, be able to create an arbitrary shape of the current and it would hence be interesting to use it to achieve other objectives. For instance torque ripple minimization.
- A very interesting approach, based on Finite State Model Predictive Control, to minimize torque ripple in a BLDC motor due to phase commutation is presented in [15]. A comparison towards lead angle adjustment would be interesting.

References

[1] A. Hughes, *Electric Motors and Drives*. Elsevier Ltd, 2006.

[2] J. Astrom, *Investigation of Issues Related to Electrical Efficiency Improvements of Pump and Fan Drives in Buildings*. PhD thesis, Department of Energy and Environment, Chalmers University of Technology, 2011.

[3] N. Mohan, T. M. Undeland, and W. P. Robbins, *Power Electronics. Converters, Applications and Design*. John Wiley & Sons, inc, 2003.

[4] S. Baldursson, "Bldc motor modelling and control - a matlab/simulink implementation," Master's thesis, Department of Energy and Environment, Chalmers University of Technology, 2005.

[5] T. Glad and L. Ljung, *Control Theory. Multivariable and Nonlinear Methods*. Taylor & Francis, 2000.

[6] L. Harnefors, "Control of variable-speed drives," tech. rep., Department of Electronics, Malardalen College University, 2002.

[7] M. Bongiorno, J. Svensson, and L. Angquist, "Online estimation of subsynchronous voltage components in power systems," tech. rep., Department of Energy and Environment, Chalmers University of Technology, ABB Power Technologies, 2008.

[8] M. Beza, "Control of energy storage equipped shunt-connected converter for electric power system stability enhancement," tech. rep., Department of Energy and Environment, Chalmers University of Technology, 2012.

[9] K. J. Astrom and B. Wittenmark, *Adaptive Control*. Addison-Wesley Publishing Company, 1995.

[10] M. Beza and M. Bongiorno, "Application of recursive least square (rls) algorithm with variable forgetting factor for frequency components estimation in a generic input signal," tech. rep., Department of Energy and Environment, Chalmers University of Technology, 2012.

[11] S.-I. Park, T.-S. Kim, S.-C. Ahn, and D.-S. Hyun, "An improved current control method for torque improvement of high-speed bldc motor," tech. rep., Hanyang University, PNA Electronics, 2003.

[12] Z. Q. Zhu, S. Bentouati, and D. Howe, "Control of single-phase permanent magnet brushless dc drives for high-speed applications," tech. rep., University of Sheffield, 2000.

[13] B.-G. Gu, J.-H. Choi, S. hyun Rhyu, and I.-S. Jung, "Optimal lead angle calculation for brushless dc motor," tech. rep., Korea Electronics Technology Institute, 2010.

[14] A. H. Niesar and A. V. H. Moghbelli, "Commutation torque ripple if four-switch, brushless dc motor drives, part ii: Controllability and minimization," tech. rep., Department of Electrical Engineering, Iran University of Science and Technology, Department of Electrical and Computer Engineering, Isfahan University of Technology, 2006.

[15] C. Xia, Y. Wang, and T. Shi, "Implementation of finite-state model predictive control for commutation torque ripple minimization of permanent-magnet brushless dc motor," tech. rep., Tianjin University, Tianjin Polytechnic University, 2012.

[16] D. Hanselman, *Brushless Permanent Magnet Motor Design*. Magna Physics Publishing, 2006.

[17] R. Carlson, M. Lajoie-Mazenc, and J. C. dos Fagundes, "Analysis of torque ripple due to phase commutation in brushless dc machines," tech. rep., Universidade Federal do Rio Grande do Sul, Laboratoire d'Electrotechnique et d'Electronique Industrielle, 1992.

[18] R. Krishnan, *Permanent Magnet Synchronous and Brushless DC Motor Drives*. Taylor and Francis Group, 2010.

Appendix A

Two axis representation of three phase systems

A.1 Transformation of three phase quantities to complex vectors

Provided that there is no zero sequence, it is evident that a three phase system constituted by the quantities v_a, v_b and v_c can be represented by an equivalent two phase system since v_a, v_b and v_c are not linearly independent.

The quantities are often transformed into a vector $v^{(\alpha\beta)}$ in a stationary complex reference frame according to

$$v^{(\alpha\beta)}(t) = v_\alpha + jv_\beta = K(v_a(t) + v_b(t)e^{j\frac{2\pi}{3}} + v_c(t)e^{j\frac{4\pi}{3}}) \tag{A.1}$$

where the constant K can be chosen to be $\sqrt{\frac{2}{3}}$ or $\frac{2}{3}$ to obtain power invariant or amplitude invariant transformation, respectively. Equation (A.1) can be expressed in matrix form as

$$\begin{bmatrix} v_\alpha \\ v_\beta \end{bmatrix} = K \begin{bmatrix} 1 & -\frac{1}{2} & -\frac{1}{2} \\ 0 & \frac{\sqrt{3}}{2} & -\frac{\sqrt{3}}{2} \end{bmatrix} \begin{bmatrix} v_a \\ v_b \\ v_c \end{bmatrix} \tag{A.2}$$

The inverse transformation is given by

$$\begin{bmatrix} v_a \\ v_b \\ v_c \end{bmatrix} = \frac{1}{K} \begin{bmatrix} \frac{2}{3} & 0 \\ -\frac{2}{3} & \frac{1}{\sqrt{3}} \\ -\frac{2}{3} & -\frac{1}{\sqrt{3}} \end{bmatrix} \begin{bmatrix} v_\alpha \\ v_\beta \end{bmatrix} \tag{A.3}$$

A.2 Transformation to rotating coordinate systems

Assume that the vector v rotates with the angular frequency ω_e in the $\alpha\beta$-system. By introducing a rotating coordinate system that rotates with the same angular frequency ω_e, the vector v will appear as a fixed vector in that coordinate system. This is visualized in Figure A.1.

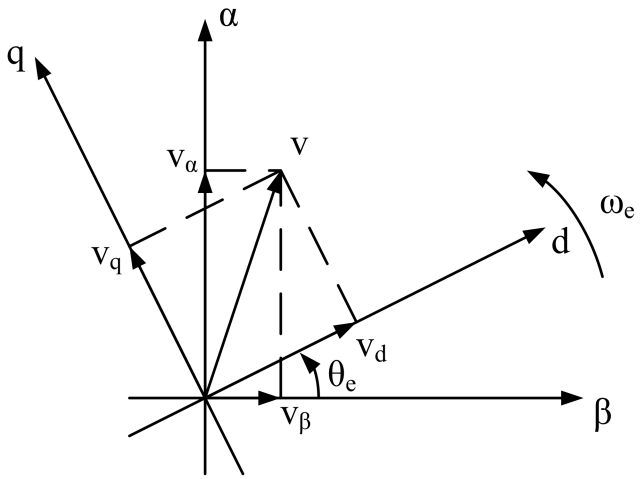

Fig. A.1 Relation between the $\alpha\beta$-coordinate system and the dq- coordinate system.

By referring to Figure A.1 it is evident that the transformation is given by

$$v^{(dq)} = v^{(\alpha\beta)} e^{-j\theta_e} \tag{A.4}$$

and the inverse transformation is given by

$$v^{(\alpha\beta)} = v^{(dq)} e^{j\theta_e} \tag{A.5}$$

The transformations A.4 and A.5 can be written in vector form as

$$\begin{bmatrix} v_d \\ v_q \end{bmatrix} = \begin{bmatrix} \cos(\theta_e) & \sin(\theta_e) \\ -\sin(\theta_e) & \cos(\theta_e) \end{bmatrix} \begin{bmatrix} v_\alpha \\ v_\beta \end{bmatrix} \tag{A.6}$$

and

$$\begin{bmatrix} v_\alpha \\ v_\beta \end{bmatrix} = \begin{bmatrix} \cos(\theta_e) & -\sin(\theta_e) \\ \sin(\theta_e) & \cos(\theta_e) \end{bmatrix} \begin{bmatrix} v_d \\ v_q \end{bmatrix} \tag{A.7}$$